Angular analysis of $B_s \to f_2'(1525)(\to K^+K^-)\mu^+\mu^-$ decays as a probe to lepton flavor universality violation

N. Rajeev,[1,*] Niladribihari Sahoo,[2,†] and Rupak Dutta[1,‡]
[1]National Institute of Technology Silchar, Silchar 788010, India
[2]Department of Physics, University of Warwick, Coventry CV4 7AL, United Kingdom

(Received 22 September 2020; accepted 11 April 2021; published 12 May 2021)

The flavor anomalies reported in R_K, R_{K^*}, P_5', and $\mathcal{B}(B_s \to \phi\mu^+\mu^-)$ indicate lepton flavor universality violation in $b \to sl^+l^-$ quark level transition decays. The deviation from the standard model prediction reported in the underlying flavor observables currently stands at the level of 2.5σ, 2.4σ, 3.3σ, and 3.7σ, respectively. In this context, we perform an angular analysis of the four-body differential decay of $B_s \to f_2'(1525)(\to K^+K^-)\mu^+\mu^-$ in a model independent effective field theory framework. The decay mode $B_s \to f_2'(1525)l^+l^-$ undergoes similar $b \to s$ neutral current quark level transition and, in principle, can provide complementary information regarding lepton flavor universality violation in $b \to sl^+l^-$ quark level transition decays. We give predictions of various physical observables such as the branching ratio, the longitudinal polarization fraction, the forward-backward asymmetry, the angular observables P_1, P_2, P_4', P_5', and also the lepton flavor sensitive observables such as the ratio of branching ratio $R_{f_2'}$, Q_{F_L}, $Q_{A_{FB}}$, Q_1, Q_2, Q_4', Q_5' for the $B_s \to f_2'(1525)(\to K^+K^-)\mu^+\mu^-$ decay mode in the standard model and in the presence of several one-dimensional and two-dimensional new physics scenarios.

DOI: 10.1103/PhysRevD.103.095007

I. INTRODUCTION

Exploring and identifying the Lorentz structure of possible new physics (NP) that lies beyond the standard model (SM) is of great importance, particularly in semileptonic B meson decays mediated via $b \to sl^+l^-$ neutral current and $b \to cl\nu$ charged current interactions. It is well known that the flavor sector could be an ideal platform to explore NP since it can provide possible indirect evidence of NP in the form of new interactions that can, in principle, be very sensitive to the existing experiments. It is also well known that, apart from the flavor sector, existence of NP is also evident from several other phenomena such as the matter/antimatter asymmetry of the universe, neutrino mass, dark matter, dark energy, and so on. In recent years, several measurements have shown hints of lepton flavor universality violation (LFUV) in the semileptonic decays of B mesons involving $b \to sl^+l^-$ ($l \in e, \mu$) neutral current and $b \to cl\nu$ ($l \in e/\mu, \tau$) charged current quark level transitions. Significant deviation from the SM expectation has been reported in various flavor observables such as R_K, R_{K^*}, P_5' in $B \to K^{(*)}l^+l^-$ decays; $\mathcal{B}(B_s \to \phi\mu^+\mu^-)$; R_D, R_{D^*}, $P_{D^*}^{\tau}$, $F_L^{D^*}$ in $B \to D^{(*)}l\nu$ decays and $R_{J/\Psi}$ in $B_c \to J/\Psi l\nu$ decays. Here we will focus mainly on the anomalies present in B meson decays mediated via $b \to sl^+l^-$ quark level transitions. The ratio of branching ratio R_K and R_{K^*} in $B \to (K, K^*)l^+l^-$ decays are defined as

$$R_{K^{(*)}} = \frac{\mathcal{B}(B \to K^{(*)}\mu^+\mu^-)}{\mathcal{B}(B \to K^{(*)}e^+e^-)}. \tag{1}$$

After the Rencontres de Moriond (2019), the current status of several observables pertaining to $b \to sl^+l^-$ quark level transition decays is as follows: the measurement of R_K from the combined data of both Run 1 and Run 2 of the LHCb Collaboration reports $R_K = 0.846^{+0.060}_{-0.054}(\text{stat})^{+0.016}_{-0.014}(\text{syst})$ [1] in the central q^2 region ($1 \le q^2 \le 6$ GeV^2), where q^2 is the invariant mass-squared of the dilepton. The deviation from the SM value of $R_K \sim 1$ [2,3] is observed to be at the level of $\sim 2.5\sigma$. Similarly, R_{K^*} was measured in two different q^2 bins by two different experiments: in the low q^2 bin ($0.045 \le q^2 \le 1.1$ GeV^2), LHCb reports $R_{K^*} = 0.660^{+0.110}_{-0.070}(\text{stat}) \pm 0.024(\text{syst})$ [4,5] and the Belle Collaboration reports $R_{K^*} = 0.52^{+0.36}_{-0.26}(\text{stat}) \pm 0.05(\text{syst})$ [6], and in the central q^2 bin ($1.1 \le q^2 \le 6$ GeV^2), LHCb reports $R_{K^*} = 0.685^{+0.113}_{-0.069}(\text{stat}) \pm 0.047(\text{syst})$ [4,5] and Belle reports $R_{K^*} = 0.96^{+0.45}_{-0.29}(\text{stat}) \pm 0.11(\text{syst})$ [6]. These measurements differ

*rajeev_rs@phy.nits.ac.in
†niladri.sahoo@warwick.ac.uk
‡rupak@phy.nits.ac.in

TABLE I. Current status of R_K and R_{K^*} and P_5' in $B \to K^{(*)} l^+ l^-$ and the branching ratio of $\mathcal{B}(B_s \to \phi\mu^+\mu^-)$.

	q^2 bins	Theoretical predictions	Experimental measurements	Deviation
R_K	[1.0, 6.0]	1 ± 0.01 [2,3]	$0.846^{+0.060}_{-0.054}\,(\text{stat})^{+0.016}_{-0.014}\,(\text{syst})$ [1]	$\sim 2.5\sigma$
R_{K^*}	[0.045, 1.1]	1 ± 0.01 [2,3]	$0.660^{+0.110}_{-0.070}\,(\text{stat}) \pm 0.024\,(\text{syst})$ [4,5]	
		1 ± 0.01 [2,3]	$0.52^{+0.36}_{-0.26}\,(\text{stat}) \pm 0.05\,(\text{syst})$ [6]	$\sim 2.4\sigma$
	[1.1, 6.0]	1 ± 0.01 [2,3]	$0.685^{+0.113}_{-0.069}\,(\text{stat}) \pm 0.047\,(\text{syst})$ [4,5]	
		1 ± 0.01 [2,3]	$0.96^{+0.45}_{-0.29}\,(\text{stat}) \pm 0.11\,(\text{syst})$ [6]	
P_5'	[4.0, 6.0]	-0.757 ± 0.074 [8]	-0.21 ± 0.15 [9–11]	$\sim 3.3\sigma$
	[4.3, 6.0]	$-0.774^{+0.0.061+0.087}_{-0.059-0.093}$ [7]	$-0.96^{+0.22}_{-0.21}\,(\text{stat}) \pm 0.16\,(\text{syst})$ [13]	$\sim 1.0\sigma$
	[4.0, 8.0]	-0.881 ± 0.082 [15]	$-0.267^{+0.275}_{-0.269}\,(\text{stat}) \pm 0.049\,(\text{syst})$ [14]	$\sim 2.1\sigma$
$\mathcal{B}(B_s \to \phi\mu^+\mu^-)$	[1.0, 6.0]	$(5.39 \pm 0.66) \times 10^{-8}$ [12,18]	$(2.57 \pm 0.37) \times 10^{-8}$ [16,17]	$\sim 3.7\sigma$

from the SM prediction of $R_{K^*} \sim 1$ [2,3] at the level of $\sim 2.4\sigma$. In addition to R_K and R_{K^*}, deviation from the SM expectation is also observed in the measurements of the angular distributions of $B \to K^*\mu^+\mu^-$, particularly in P_5' [7,8]. The ATLAS [9] and LHCb [10,11] Collaborations measured P_5' in the bin $q^2 \in [4, 6]$ GeV^2 and they differ by $\sim 3.3\sigma$ [12] from the SM expectation [8]. Similarly, the CMS [13] measurement in $q^2 \in [4.3, 6]$ GeV^2 and the Belle [14] measurement in $q^2 \in [4.3, 8]$ GeV^2 differ by 1σ and 2.1σ, respectively, from the SM expectations [7,15]. Moreover, the measured value of the branching ratio $\mathcal{B}(B_s \to \phi\mu^+\mu^-)$ [16,17] is found to deviate at the level of $\sim 3.7\sigma$ from the SM expectations [12,18]. In Table I we report the current status of R_K, R_{K^*}, P_5', and $\mathcal{B}(B_s \to \phi\mu^+\mu^-)$. At present, the dedicated ongoing B factory programs at Belle II and LHCb emerge as promising platforms that can either confirm or refute the existence of NP in $b \to s l^+ l^-$ transition decays.

Our main aim is to study the impact of NP on $B_s \to f_2'(1525)\mu^+\mu^-$ decay observables in a model independent effective theory formalism. The $B_s \to f_2'(1525)\mu^+\mu^-$ decay mode has received less attention both from the theoretical and the experimental side and it has not been discussed earlier in detail. Although, in Ref. [19], the authors discussed the SM results for both the μ mode and τ mode of $B_s \to f_2'(1525) l^+ l^-$ along with the $B \to K_2^*(1430) l^+ l^-$ decays, more emphasis was given to $B \to K_2^*$ rather than $B_s \to f_2'$ decays. Also, the branching ratio of f_2' decaying into K^+K^- was not considered in their numerical analysis. In Ref. [19], the authors also discussed the impact of NP on several observables coming from two different NP models, such as the vectorlike quark model and the family nonuniversal Z' model. Similarly, there is an ample number of literatures discussing the $B \to K_2^*(1430) l^+ l^-$ decays [20–27] mediated via the same $b \to s l^+ l^-$ quark level transition.

So far we don't have many experimental results on electroweak penguin decays involving spin 2 particles. The experimental techniques used for $B_s \to \phi l^+ l^-$ can be adjusted to the $B_s \to f_2'(1525) l^+ l^-$ decay as well, because both ϕ and $f_2'(1525)$ decay to a pair of charged kaons which are easily detected by the LHCb detector. Since the dominating structures in the K^+K^- spectrum are the P wave $\phi(1020)$, and there are several possible resonances around 1500 MeV$/c^2$, it is natural to look at this regime to study. Furthermore, the presence of D waves in this mass region yields a richer spectrum for exploring interesting angular observables.

Although there are other resonances like $f_2(1270)$ and $f_0(1500)$ between $\phi(1020)$ and $f_2'(1525)$, they have a smaller branching fraction of 5% or less into the K^+K^- final state and are very unlikely to have large rates. Hence, $f_2'(1525)$ is the best option after $\phi(1020)$ [28]. This decay in the muonic mode can be observed with the currently available data and we expect around 200 events for this mode. The currently available data is statistically limited for performing angular analysis; the branching fraction measurement is only possible claiming the first observation of this decay in muonic mode. With more data in Run 3, the measurement of angular observables is possible. In the published Run 1 angular analysis of $B_s \to \phi\mu^+\mu^-$ decays [17], we see 10–20% statistical uncertainties across all angular observables. So far, no results have been published with the full Run 1 and Run 2 data. We expect the statistical uncertainty in case of full Run 1 + Run 2 analysis to go down by a factor of 40%, which means 5–10% total statistical uncertainty for angular observables in case of $B_s \to \phi\mu^+\mu^-$ decays with full Run 1 + Run 2 data. For $B_s \to f_2'(1525)\mu^+\mu^-$, we expect the statistical uncertainty to be three times more with respect to $B_s \to \phi\mu^+\mu^-$ decays, i.e., 15–30% statistical error.

The present paper is organized as follows: in Sec. II, we start with a brief overview of the effective Hamiltonian for $b \to s l^+ l^-$ quark level transition decays in the presence of new vector and axial vector NP operators. A brief discussion of $B_s \to f_2'$ hadronic matrix elements, followed by the angular distribution and the transversity amplitudes for

$B_s \to f_2'(1525)(\to K^+K^-)\mu^+\mu^-$ decays, are also reported. Finally we write down the decay distribution and expressions for several lepton flavor universal (LFU) observables. In Sec. III, we report our results that are obtained in the SM and in several NP scenarios. We conclude with a brief summary of our results in Sec. IV.

II. THEORETICAL FRAMEWORK

A. Effective Hamiltonian

The effective Hamiltonian for $b \to s l^+ l^-$ quark level transition decays in the presence of new vector and axial vector NP operators is written as

$$\begin{aligned}\mathcal{H}_{\rm eff} = &-\frac{G_F}{\sqrt{2}} V_{tb} V_{ts}^* \frac{\alpha_e}{4\pi}\Big[C_9^{\rm eff}\bar{s}\gamma^\mu P_L b\bar{l}\gamma_\mu l + C_{10}^{\rm eff}\bar{s}\gamma^\mu P_L b\bar{l}\gamma_\mu\gamma_5 l \\ &-\frac{2m_b}{q^2} C_7^{\rm eff}\bar{s} i q_\nu \sigma^{\mu\nu} P_R b\bar{l}\gamma_\mu l + C_9^{\rm NP}\bar{s}\gamma^\mu P_L b\bar{l}\gamma_\mu l \\ &+ C_{10}^{\rm NP}\bar{s}\gamma^\mu P_L b\bar{l}\gamma_\mu\gamma_5 l + C_9'\bar{s}\gamma^\mu P_R b\bar{l}\gamma_\mu l \\ &+ C_{10}'\bar{s}\gamma^\mu P_R b\bar{l}\gamma_\mu\gamma_5 l\Big], \end{aligned} \tag{2}$$

where G_F is the Fermi coupling constant, α_e is the fine structure constant, V_{tb} and V_{ts} are the corresponding Cabibbo-Kobayashi-Maskawa (CKM) matrix elements, and $P_{L,R} = (1 \mp \gamma_5)/2$. The factorizable loop terms are incorporated within the effective Wilson coefficients (WCs) $C_7^{\rm eff}$ and $C_9^{\rm eff}$ as [29]

$$\begin{aligned} C_7^{\rm eff} &= C_7 - \frac{C_5}{3} - C_6, \\ C_9^{\rm eff} &= C_9(\mu) + h(\hat{m}_c, \hat{s}) C_0 \\ &\quad -\frac{1}{2}h(1,\hat{s})(4C_3 + 4C_4 + 3C_5 + C_6) \\ &\quad -\frac{1}{2}h(0,\hat{s})(C_3 + 3C_4) + \frac{2}{9}(3C_3 + C_4 + 3C_5 + C_6), \end{aligned} \tag{3}$$

where $\hat{s} = q^2/m_b^2$, $\hat{m}_c = m_c/m_b$, and $C_0 = 3C_1 + C_2 + 3C_3 + C_4 + 3C_5 + C_6$. Similarly, the auxiliary functions are defined as

$$\begin{aligned} h(z,\hat{s}) = &-\frac{8}{9}\ln\frac{m_b}{\mu} - \frac{8}{9}\ln z + \frac{8}{27} + \frac{4}{9}x - \frac{2}{9}(2+x)|1-x|^{1/2} \\ &\times \begin{cases} \ln\left|\dfrac{\sqrt{1-x}+1}{\sqrt{1-x}-1}\right| - i\pi, & \text{for } x \equiv \frac{4z^2}{\hat{s}} < 1 \\ 2\arctan\dfrac{1}{\sqrt{x-1}}, & \text{for } x \equiv \frac{4z^2}{\hat{s}} > 1 \end{cases} \end{aligned} \tag{4}$$

$$h(0,\hat{s}) = -\frac{8}{9}\ln\frac{m_b}{\mu} - \frac{4}{9}\ln\hat{s} + \frac{8}{27} + \frac{4}{9}i\pi. \tag{5}$$

The additional terms in the $C_9^{\rm eff}$ describe the short distance contributions from the four-quark operators which lie away from the $c\bar{c}$ resonance region. Similarly, the long distance contributions which include the resonant state from $b \to c\bar{c}s$ which further annihilate into a lepton pair are excluded in the present analysis. Hence, we only concentrate on the regions from $q^2 \in [0.045, 0.98]$ and $q^2 \in [1.1, 6.0]$[1] GeV^2. It not necessary that the nonlocal effects are accounted only for the resonant states but also they are very important even below the charmonium contribution. This has been studied in detail in Refs. [30–33]. The authors in [30] report that, due to the virtual photon propagator, the nonfactorizable contributions to ΔC_9 are enhanced at small q^2, i.e., at $q^2 \gg 4m_l^2$. The factorizable soft gluon part $\Delta C_9(q^2)$ plays an important role in $B \to K^*$ decays. The charm loop corrections $\Delta C_9(q^2)$ almost reach up to 20% of C_9 at $1 \le q^2 \le 4$ GeV^2 in $B \to K^* ll$ decays and similarly, will not exceed more than 5% in the $B \to K ll$ decays. These nonfactorizable contributions significantly affect the differential width and the forward-backward asymmetry in $B \to K^*$ decays. The zero crossing of the forward-backward asymmetry will be effected significantly in discriminating the new physics contributions. Similarly, the nonlocal contributions in $B \to K^*$ and $B_s \to \phi$ decays have also been discussed very recently in [33]. The authors in this particular paper proposed a modified analytic parametrization of nonlocal matrix elements. These effects in fact enter the decay amplitudes in the form of nonperturbative nonlocal matrix elements which are difficult to calculate with controlled uncertainties. The recalculations of beyond the operator product expansion contributions involve the light cone sum rule and the full set of B meson light cone distribution amplitudes. In most of the theoretical papers which try to address the LFU violation in $b \to s l^+ l^-$ decays the hadronic nonlocal effects are neglected. Hence, we do not consider these corrections in our present analysis.

The new physics WCs in the effective Hamiltonian, such as $C_{9,10}^{\rm NP}$ and $C_{9,10}'$, include the effects coming from the new vector and axial vector NP couplings. In SM, all these new WCs are considered to be zero. In principle, one can have the new scalar, pseudoscalar, and tensor NP WCs, but they are severely constrained by $B_s \to \mu^+\mu^-$ and $b \to s\gamma$ measurements [34–36]. The values for each WC obtained in the leading logarithmic approximation at the energy scale $\mu = m_{b,\rm pole}$ are reported in Table III. Similarly, the values of new WCs are obtained from the global fits of Ref. [37].

[1]The $q^2 \in [0.98, 1.1]$ GeV^2 is excluded because of $\phi(1020) \to \mu^+\mu^-$ decays.

B. Spin 2 polarization tensor and $B_s \to f_2'$ hadronic matrix elements

1. Spin 2 polarization tensor

A spin 2 polarization tensor $\epsilon^{\mu\nu}(n)$, where $n \in \pm 2, \pm 1, 0$, can be constructed via a spin 1 polarization vector [19,40,41]. For the f_2' meson having the four momentum $(|\vec{p}_{f_2'}|, 0, 0, E_{f_2'})$, where $\vec{p}_{f_2'}$ and $E_{f_2'}$ are the momentum and energy of f_2' in the B_s meson rest frame, the explicit structure of polarization tensor $\epsilon^{\mu\nu}(n)$ in the ordinary coordinate frame are constructed out of a massive vector state by the use of an appropriate Clebsch-Gordan coefficients. Those are

$$\begin{aligned}
\epsilon_{\mu\nu}(\pm 2) &= \epsilon_\mu(\pm)\epsilon_\nu(\pm), \\
\epsilon_{\mu\nu}(\pm 1) &= \frac{1}{\sqrt{2}}[\epsilon_\mu(\pm)\epsilon_\nu(0) + \epsilon_\nu(\pm)\epsilon_\mu(0)], \\
\epsilon_{\mu\nu}(0) &= \frac{1}{\sqrt{6}}[\epsilon_\mu(+)\epsilon_\nu(-) + \epsilon_\nu(+)\epsilon_\mu(-)] + \sqrt{\frac{2}{3}}\epsilon_\mu(0)\epsilon_\nu(0),
\end{aligned} \tag{6}$$

where

$$\epsilon_\mu(0) = \frac{1}{m_{f_2'}}(|\vec{p}_{f_2'}|, 0, 0, E_{f_2'}), \qquad \epsilon_\mu(\pm) = \frac{1}{\sqrt{2}}(0, \mp 1, -i, 0). \tag{7}$$

In the $B_s \to f_2'(1525)l^+l^-$ decay, the $n = \pm 2$ helicity states of the f_2' are not aware of the two leptons that are obtained in the final state. Hence, it would be convenient to introduce a new polarization vector $\epsilon_{T_\mu}(h)$ as

$$\epsilon_{T_\mu}(h) = \frac{1}{m_b}\epsilon_{\mu\nu}(h)P^\nu_{B_s}, \tag{8}$$

where P_{B_s} is the four momentum of B_s meson. The polarization vector $\epsilon_{T_\mu}(h)$ satisfies the following equations [190]:

$$\begin{aligned}
\epsilon_{T_\mu}(\pm 2) &= 0, \\
\epsilon_{T_\mu}(\pm 1) &= \frac{1}{m_{B_s}}\frac{1}{\sqrt{2}}\epsilon(0)\cdot P_{B_s}\epsilon_\mu(\pm) = \frac{\sqrt{\lambda}}{\sqrt{8}m_{B_s}m_{f_2'}}\epsilon_\mu(\pm), \\
\epsilon_{T_\mu}(0) &= \frac{1}{m_{B_s}}\sqrt{\frac{2}{3}}\epsilon(0)\cdot P_{B_s}\epsilon_\mu(0) = \frac{\sqrt{\lambda}}{\sqrt{6}m_{B_s}m_{f_2'}}\epsilon_\mu(0).
\end{aligned} \tag{9}$$

2. $B_s \to f_2'$ hadronic matrix elements

Normally, for calculating the $B_s \to f_2'(1525)$ form factors, the $f_2'(1525)$ is treated to be stable and contributes as a single particle. This means that it has a simple pole at $k^2 = m^2_{f_2'(1525)}$. If there are any further higher order states, the hadronic representation goes beyond the single pole. The purpose of implementing the narrow width limit can be done by calculating the sum rules for the K^+K^- states. Recently, there have been few improvements in the theoretical predictions as of the local and nonlocal form factors are concerned. In the propagation of the intermediate strange meson, the width effect of f_2' could be important. This is because of the fact that $\Gamma_{f_2'} \gg \Gamma_\phi$. Hence, the narrow width approximation may not work well for the f_2' case, unlike ϕ. The finite-width effects which lead to 10% corrections to the form factors, which further lead to 20% corrections to the branching fractions in the case of ρ and K^*, are studied in detail in Refs. [42,43]. Nevertheless, we do not consider these effects in the present analysis. Although the corrections tend to increase the discrepancy between the SM predictions of the branching fractions and the corresponding LHCb measurements, the normalized angular observables such as P_5' and other LFU sensitive ratios, which mainly depend on the form factors, are insensitive to the finite-width corrections. Moreover, the global fit results including all these corrections are still awaited [43,44].

In general, the $B_s \to f_2'$ hadronic matrix elements can be parametrized in terms of several form factors, as follows [19,22,23,41,45]:

$$\begin{aligned}
\langle f_2'(P_{f_2'},\epsilon)|\bar{s}\gamma^\mu b|\bar{B}_s(P_{B_s})\rangle &= -\frac{2V(q^2)}{m_{B_s}+m_{f_2'}}\epsilon^{\mu\nu\rho\sigma}\epsilon^*_{T_\nu}P_{B_s\rho}P_{f_2'\sigma}, \\
\langle f_2'(P_{f_2'},\epsilon)|\bar{s}\gamma^\mu\gamma_5 b|\bar{B}_s(P_{B_s})\rangle &= 2im_{f_2'}A_0(q^2)\frac{\epsilon^*_T\cdot q}{q^2}q^\mu + i(m_{B_s}+m_{f_2'})A_1(q^2)\left[\epsilon^*_{T_\mu} - \frac{\epsilon^*_T\cdot q}{q^2}q^\mu\right] \\
&\quad - iA_2(q^2)\frac{\epsilon^*_T\cdot q}{m_{B_s}+m_{f_2'}}\left[P^\mu - \frac{m^2_{B_s}+m^2_{f_2'}}{q^2}q^\mu\right], \\
\langle f_2'(P_{f_2'},\epsilon)|\bar{s}\sigma^{\mu\nu}q_\nu b|\bar{B}_s(P_{B_s})\rangle &= -2iT_1(q^2)\epsilon^{\mu\nu\rho\sigma}\epsilon^*_{T_\nu}P_{B_s\rho}P_{f_2'\sigma}, \\
\langle f_2'(P_{f_2'},\epsilon)|\bar{s}\sigma^{\mu\nu}\gamma_5 q_\nu b|\bar{B}_s(P_{B_s})\rangle &= T_2(q^2)[(m^2_{B_s}+m^2_{f_2'})\epsilon_{T_\mu}\epsilon^*_T\cdot qP^\mu] + T_3(q^2)\epsilon^*_T\cdot q\left[q^\mu - \frac{q^2}{m^2_{B_s}+m^2_{f_2'}}P^\mu\right],
\end{aligned} \tag{10}$$

where P_{B_s} and $P_{f_2'}$ are the four momenta of the B_s meson and f_2', respectively, and $q = P_{B_s} - P_{f_2'}$. In general, the $B_s \to f_2'$ transition form factors are nonperturbative in nature and they can be calculated using several nonperturbative approaches. We follow Ref. [41] and write the $B_s \to f_2'$ transition form factors as

$$F(q^2) = \frac{F(0)}{(1-q^2/m_{B_s}^2)[1-a(q^2/m_{B_s}^2)+b(q^2/m_{B_s}^2)^2]}, \quad (11)$$

where F denotes A_0, A_1, V, T_1, T_2, and T_3, respectively. Similarly, A_2 is related to A_0 and A_1 by

$$A_2(q^2) = \frac{m_{B_s}+m_{f_2'}}{m_{B_s}^2-q^2}[(m_{B_s}+m_{f_2'})A_1(q^2) - 2m_{f_2'}A_0(q^2)]. \quad (12)$$

The numerical entries of the $B_s \to f_2'$ form factors at the maximum recoil point and the two fitted parameters a and b are reported in Table IV.

The $B \to T$ form factors contain one more pole structure in the q^2 distribution and they are expected to be sharper than the $B \to V$ form factors. But the parametrization of $B \to T$ form factors is analogous to $B \to V$ form factors and the only difference is the replacement of ϵ by ϵ_T. This can be easily related when we mark the pole at $q^2 = 0$ and we get the relation $2m_T A_0(0) = (m_{B_s}+m_T)A_1(0) - (m_{B_s}-m_T)A_2(0)$, which has a similar relation as of the $B \to V$ case.

The Lorentz structures of the wave functions and the B decay form factors involving the vector and tensor mesons have great similarities. Hence this allows us to obtain the factorization formulas of $B \to T$ form factors from $B \to V$ ones. Further, the two set of $B \to V$ and $B \to T$ form factors have the same signs and related q^2 dependency. This is because the light cone distribution amplitudes of the tensor mesons and the vector mesons have similar shapes in the dominant region of the perterbative quantum chromodynamics (pQCD) approach. In the pQCD, the factorization formula is given by [41]

$$\mathcal{M} = \int_0^1 dx_1 dx_2 \int d^2\vec{b}_1 d^2\vec{b}_2 \phi_B(x_1,\vec{b}_1,P_B,t) \times T_x(x_1,x_2,\vec{b}_1,\vec{b}_1,t)\phi_2(x_2,\vec{b}_2,P_2,t)S_t(x_2) \times \exp[-S_B(t)-S_2(t)]. \quad (13)$$

This has been generalized to the number of transition form factors for various final state mesons including scalar, vector, pseudoscalar, and axial-vector mesons. The correspondence between vector and tensor mesons are obtained in a comparative way. Both light cone distribution amplitudes (LCDAs) of the tensor meson and $B \to T$ form factors coincide with the quantities involving a vector meson as

$$\phi_V^{(i)} \leftrightarrow \phi_T^{(i)}, \qquad F^{B\to T} \leftrightarrow F^{B\to V}, \quad (14)$$

where F and $\phi_{V,T}^{(i)}$ represent the $B \to (T,V)$ form factors and LCDA respectively. The polarization vector ϵ is replaced by $\epsilon_\bullet$ and ϵ_T, respectively, in the LCDAs and in the transition form factors. As a result, the $B \to T$ form factors are factorized as

$$F^{B\to T}(\phi_T^{(i)}) = \frac{\epsilon_\bullet}{\epsilon_T}F^{B\to V}(\phi_V^{(i)}) = \frac{2m_B m_T}{m_B^2-q^2}F^{B\to V}(\phi_V^{(i)}). \quad (15)$$

While extracting the form factors in a nonperturbative way by using QCD sum rules, the pole structure of the form factors are constrained in an analytic way whereas, in pQCD platform, which uses the perturbative properties of the form factors such as the factorization, construct the parametrization form in a phenomenological way. In general, the polar form of $B \to V$ form factors include pole form, dipole form, exponential form, and the BK parametrization [46]. By adopting this approach one defines the dipole form of $B \to V$ form factors in a pQCD as

$$F(q^2) = \frac{F(0)}{1-a(q^2/m_B^2)+b(q^2/m_B^2)^2}. \quad (16)$$

The only difference for the case of $B \to T$ form factors is that it receives an additional q^2 dependency. This can be seen in the factorization formula of Eq. (15) and the formula for $F(q^2)$ in Eq. (11). Hence, this modification is appropriate for the q^2 distribution of $B \to T$ form factors. We refer to Ref. [41] for all the omitted details.

C. Angular distribution and the transversity amplitudes for $B_s \to f_2'(1525)(\to K^+K^-)\mu^+\mu^-$ decays

The decay amplitude for $B_s \to f_2'(1525)l^+l^-$ can be obtained from the effective Hamiltonian of Eq. (2). Using the helicity techniques of Ref. [19], the differential decay width of the four-body decay of $B_s \to f_2'(1525)(\to K^+K^-)\mu^+\mu^-$ can be written in terms of several angular coefficients as

$$\frac{d^4\Gamma}{dq^2 d\cos\theta_K d\cos\theta_l d\phi} = \frac{3}{8}[I_1^c C^2 + 2I_1^s S^2 + (I_2^c C^2 + 2I_2^s S^2)\cos 2\theta_l + 2I_3 S^2 \sin^2\theta_l \cos 2\phi + 2\sqrt{2} I_4 CS \sin 2\theta_l \cos\phi + 2\sqrt{2} I_5 CS \sin\theta_l \cos\phi + 2I_6 S^2 \cos\theta_l + 2\sqrt{2} I_7 CS \sin\theta_l \sin\phi + 2\sqrt{2} I_8 CS \sin 2\theta_l \sin\phi + 2I_9 S^2 \sin^2\theta_l \sin 2\phi], \quad (17)$$

where $C = C(f_2') \equiv \sqrt{\frac{5}{16\pi}}(3\cos^2\theta_K - 1)$ and $S = S(f_2') \equiv \sqrt{\frac{15}{32\pi}}\sin(2\theta_K)$. The direction of f_2' is chosen along the z direction in the B_s meson rest frame. The polar angle $\theta_K(\theta_l)$ is defined as the angle between the direction of $K^-(\mu^-)$ and the z axis in the rest frame of the lepton pair. Similarly, ϕ is the angle between the decay planes of f_2' and the lepton pair. Moreover, the angular coefficients $I_i(q^2)$ are defined as

$$\begin{aligned}
I_1^c &= (|A_{L0}|^2 + |A_{R0}|^2) + 8\frac{m_l^2}{q^2}\mathrm{Re}[A_{L0}A_{R0}^*] + 4\frac{m_l^2}{q^2}|A_t|^2,\\
I_2^c &= -\beta_l^2(|A_{L0}|^2 + |A_{R0}|^2),\\
I_1^s &= \frac{3}{4}[|A_{L\perp}|^2 + |A_{L\parallel}|^2 + |A_{R\perp}|^2 + |A_{R\parallel}|^2]\left(1 - \frac{4m_l^2}{3q^2}\right) + \frac{4m_l^2}{q^2}\mathrm{Re}[A_{L\perp}A_{R\perp}^* + A_{L\parallel}A_{R\parallel}^*],\\
I_2^s &= \frac{1}{4}\beta_l^2[|A_{L\perp}|^2 + |A_{L\parallel}|^2 + |A_{R\perp}|^2 + |A_{R\parallel}|^2],\\
I_3 &= \frac{1}{2}\beta_l^2[|A_{L\perp}|^2 - |A_{L\parallel}|^2 + |A_{R\perp}|^2 - |A_{R\parallel}|^2],\\
I_4 &= \frac{1}{\sqrt{2}}\beta_l^2[\mathrm{Re}(A_{L0}A_{L\parallel}^*) + \mathrm{Re}(A_{R0}A_{R\parallel}^*)],\\
I_5 &= \sqrt{2}\beta_l[\mathrm{Re}(A_{L0}A_{L\perp}^*) - \mathrm{Re}(A_{R0}A_{R\perp}^*)],\\
I_6 &= 2\beta_l[\mathrm{Re}(A_{L\parallel}A_{L\perp}^*) - \mathrm{Re}(A_{R\parallel}A_{R\perp}^*)],\\
I_7 &= \sqrt{2}\beta_l[\mathrm{Im}(A_{L0}A_{L\parallel}^*) - \mathrm{Im}(A_{R0}A_{R\parallel}^*)],\\
I_8 &= \frac{1}{\sqrt{2}}\beta_l^2[\mathrm{Im}(A_{L0}A_{L\perp}^*) + \mathrm{Im}(A_{R0}A_{R\perp}^*)],\\
I_9 &= \beta_l^2[\mathrm{Im}(A_{L\parallel}A_{L\perp}^*) + \mathrm{Im}(A_{R\parallel}A_{R\perp}^*)], \quad (18)
\end{aligned}$$

where $\beta_l = \sqrt{1 - 4m_l^2/q^2}$ is the mass correction factor. In our analysis, we assume all the angular coefficients to be real and CP conserving. For convenience, we introduce here the transversity amplitudes A_{L0}, A_{R0}, $A_{L\perp}$, $A_{R\perp}$, $A_{L\parallel}$, and $A_{R\parallel}$. However, they are nothing but linear combinations of the helicity amplitudes as mentioned in Ref. [19]. The subscripts L and R represent the chiralities of the lepton current where the right chiral amplitudes differ by left chiral amplitudes as $A_{Ri} = A_{Li}|_{C_{10}\to -C_{10}}$. The amplitudes A_i are obtained from the hadronic $B_s \to f_2' V$ amplitudes $\mathcal{H}_i$ through $A_i = \sqrt{\frac{\sqrt{\lambda}q^2\beta_l \mathcal{B}(f_2'(1525)\to K^+K^-)}{3\cdot 32 m_B^3 \pi^3}}\mathcal{H}_i$. The details of the helicity amplitudes are discussed in Appendix B. The explicit expressions for the transversity amplitudes for the $B_s \to f_2'(1525)(\to K^+K^-)\mu^+\mu^-$ decay are written as follows:

$$\begin{aligned}
A_{L0} &= N_{f_2'}\frac{\sqrt{\lambda}}{\sqrt{6}m_{B_s}m_{f_2'}}\frac{1}{2m_{f_2'}\sqrt{q^2}} \times \left\{(C_9^{\mathrm{eff}} - C_{10})\left[(m_{B_s}^2 - m_{f_2'}^2 - q^2)(m_{B_s} + m_{f_2'})A_1 - \frac{\lambda}{m_{B_s} + m_{f_2'}}A_2\right] + 2m_b C_7^{\mathrm{eff}}\left[(m_{B_s}^2 + 3m_{f_2'}^2 - q^2)T_2 - \frac{\lambda}{m_{B_s}^2 - m_{f_2'}^2}T_3\right]\right\},\\
A_{L\perp} &= -N_{f_2'}\sqrt{2}\frac{\sqrt{\lambda}}{\sqrt{8}m_{B_s}m_{f_2'}}\left[(C_9^{\mathrm{eff}} - C_{10})\frac{\sqrt{\lambda}}{m_{B_s} + m_{f_2'}}V + \frac{\sqrt{\lambda}2m_b C_7^{\mathrm{eff}}}{q^2}T_1\right],\\
A_{L\parallel} &= N_{f_2'}\sqrt{2}\frac{\sqrt{\lambda}}{\sqrt{8}m_{B_s}m_{f_2'}}\left[(C_9^{\mathrm{eff}} - C_{10})(m_{B_s} + m_{f_2'})A_1 + \frac{2m_b C_7^{\mathrm{eff}}(m_{B_s}^2 - m_{f_2'}^2)}{q^2}T_2\right],\\
A_{Lt} &= N_{f_2'}\frac{\sqrt{\lambda}}{\sqrt{6}m_{B_s}m_{f_2'}}(C_9^{\mathrm{eff}} - C_{10})\frac{\sqrt{\lambda}}{\sqrt{q^2}}A_0, \quad (19)
\end{aligned}$$

where $\lambda = m_{B_s}^4 + m_{f_2'}^4 + q^4 - 2(m_{B_s}^2 m_{f_2'}^2 + m_{f_2'}^2 q^2 + q^2 m_{B_s}^2)$ and $N_{f_2'}$ is the normalization constant defined as

$$N_{f_2'} = \left[\frac{G_F^2\alpha_{em}^2}{3\cdot 2^{10}\pi^5 m_{B_s}^3}|V_{tb}V_{ts}^*|^2 q^2\sqrt{\lambda}\left(1 - \frac{4m_l^2}{q^2}\right)^{1/2} \times \mathcal{B}(f_2' \to K^+K^-)\right]^{1/2}. \quad (20)$$

D. Decay distribution and LFU observables

By integrating Eq. (17) with respect to θ_K, θ_l, and ϕ, we obtain the differential decay rate,

$$\frac{d\Gamma}{dq^2} = \frac{1}{4}[3I_1^c + 6I_1^s - I_2^c - 2I_2^s]. \tag{21}$$

We define several other q^2 dependent observables such as the differential branching ratio, the longitudinal polarization fraction, and the forward-backward asymmetry for the $B_s \to f_2'(1525)(\to K^+K^-)\mu^+\mu^-$ decays. Those are:

$$\mathrm{DBR}(q^2) = \frac{d\Gamma/dq^2}{\Gamma_{\mathrm{Total}}}, \quad F_L(q^2) = \frac{3I_1^c - I_2^c}{3I_1^c + 6I_1^s - I_2^c - 2I_2^s},$$
$$A_{FB}(q^2) = \frac{3I_6}{3I_1^c + 6I_1^s - I_2^c - 2I_2^s}. \tag{22}$$

In principle, the angular analysis of the $B_s \to f_2'(1525)(\to K^+K^-)\mu^+\mu^-$ decay provides several additional observables in the form of ratios of various angular coefficients. These observables are found to be very sensitive to NP. Here we define some angular observables such as $\langle P_1\rangle$, $\langle P_2\rangle$, $\langle P_4'\rangle$, and $\langle P_5'\rangle$, as reported in Refs. [7,8]. The explicit expressions are as follows:

$$\langle P_1\rangle = \frac{1}{2}\frac{\int_{\mathrm{bin}} dq^2 I_3}{\int_{\mathrm{bin}} dq^2 I_2^s}, \quad \langle P_2\rangle = \frac{1}{8}\frac{\int_{\mathrm{bin}} dq^2 I_6}{\int_{\mathrm{bin}} dq^2 I_2^s},$$
$$\langle P_4'\rangle = \frac{\int_{\mathrm{bin}} dq^2 I_4}{\sqrt{-\int_{\mathrm{bin}} dq^2 I_2^c \int_{\mathrm{bin}} dq^2 I_2^s}},$$
$$\langle P_5'\rangle = \frac{\int_{\mathrm{bin}} dq^2 I_5}{2\sqrt{-\int_{\mathrm{bin}} dq^2 I_2^c \int_{\mathrm{bin}} dq^2 I_2^s}}. \tag{23}$$

One can construct several other observables that can be defined in the form of ratios or in the form of differences between the observables involving two different families of lepton pairs. These observables, such as the ratio of branching ratio $R_{f_2'}$ and $\langle Q_{F_L}\rangle$, $\langle Q_{A_{FB}}\rangle$, $\langle Q_i^{(\prime)}\rangle$ ($i \in 1, 2, 4, 5$), are quite sensitive to NP. In the SM, we expect the value of $R_{f_2'}$ to be very close to 1. Similarly, since the observables $Q^{(\prime)}$ [47] are defined to be the differences between the e and μ modes, one would expect these quantities to be almost zero in the SM. Hence any deviation from zero would be a clear signal of NP in $b \to sl^+l^-$ quark level transition decays. Measurement of these observables in the future may provide crucial information regarding LFUV observed in various B meson decays. The explicit expressions for these observables are as follows:

$$R_{f_2'}(q^2) = \frac{\mathcal{B}(B_s \to f_2'\mu^+\mu^-)}{\mathcal{B}(B_s \to f_2' e^+e^-)}, \tag{24}$$

and

$$\langle Q_{F_L}\rangle = \langle {F_L}^{\mu}\rangle - \langle {F_L}^{e}\rangle, \qquad \langle Q_{A_{FB}}\rangle = \langle {A_{FB}}^{\mu}\rangle - \langle {A_{FB}}^{e}\rangle,$$
$$\langle Q_i^{(\prime)}\rangle = \langle P_i^{(\prime)\mu}\rangle - \langle P_i^{(\prime)e}\rangle. \tag{25}$$

III. RESULTS AND DISCUSSIONS

A. Input parameters

We report here all the relevant input parameters that are used in our numerical analysis. In Table II we report the masses of the mesons, leptons, and quarks in GeV, the Fermi coupling constant in GeV^{-2}, and the lifetime of B_s meson in seconds. We consider the masses of the b quark and c quark evaluated at the $\overline{\mathrm{MS}}$ scheme. The uncertainties associated with the CKM matrix element and $\mathcal{B}(f_2' \to K^+K^-)$ are reported within parentheses. We do not report the uncertainties associated with other input parameters as they are not important for our analysis. In Table III, we report the values of Wilson coefficients $C_i(m_b)$ that are evaluated in the leading logarithmic approximation. The form factor input parameters evaluated in the pQCD approach are reported in Table IV where $F(0)$ denote

TABLE II. Theory input parameters [38].

Parameter	Value	Parameter	Value	Parameter	Value	Parameter	Value	Parameter	Value
m_{B_s}	5.36689	$m_{f_2'}$	1.525	$m_b^{\overline{\mathrm{MS}}}$	4.20	$m_c^{\overline{\mathrm{MS}}}$	1.28	m_b^{pole}	4.80
τ_{B_s}	1.509×10^{-12}	G_F	1.1663787×10^{-5}	α_e	1/133.28	$\lvert V_{tb}V_{ts}^*\rvert$	0.04088(55)	$\mathcal{B}(f_2' \to K^+K^-)$	0.4435(11)

TABLE III. Wilson coefficients $C_i(m_b)$ in the leading logarithmic approximation [39].

C_1	C_2	C_3	C_4	C_5	C_6	C_7^{eff}	C_9	C_{10}
−0.248	1.107	0.011	−0.026	0.007	−0.031	−0.313	4.344	−4.669

TABLE IV. Form factor input parameters [41].

	V	A_0	A_1	T_1	T_2	T_3
$F(0)$	$0.20^{+0.04+0.05}_{-0.03-0.03}$	$0.16^{0.03+0.03}_{-0.02-0.02}$	$0.12^{+0.02+0.03}_{-0.02-0.02}$	$0.16^{+0.03+0.04}_{-0.03-0.02}$	$0.16^{+0.03+0.04}_{-0.03-0.02}$	$0.13^{+0.03+0.03}_{-0.02-0.02}$
a	$1.75^{+0.02+0.05}_{-0.00-0.03}$	$1.69^{+0.00+0.04}_{-0.01-0.03}$	$0.80^{+0.02+0.07}_{-0.00-0.03}$	$1.75^{+0.01+0.05}_{-0.00-0.05}$	$0.82^{+0.00+0.04}_{-0.04-0.06}$	$1.64^{+0.02+0.06}_{-0.00-0.06}$
b	$0.69^{+0.05+0.08}_{-0.01-0.01}$	$0.64^{+0.00+0.01}_{-0.04-0.02}$	$-0.11^{+0.05+0.06}_{-0.00-0.00}$	$0.71^{+0.03+0.06}_{-0.01-0.08}$	$-0.08^{+0.00+0.03}_{-0.09-0.08}$	$0.57^{+0.04+0.05}_{-0.01-0.09}$

the form factors at $q^2 = 0$, i.e., at the maximum recoil point, and a and b are the two fitted parameters. There are two kinds of errors associated with $F(0)$, a and b. The first error is coming from the decay constant of the B_s meson and the shape parameter ω_b and the second error is coming from the $\Lambda_{\rm QCD}$, the scales ts, and the threshold resummation parameter c. We refer to Ref. [41] for all the omitted details.

B. Standard model predictions

We now proceed to discuss our results in the SM. We report in Tables V and VI the central values and the corresponding 1σ uncertainties for each of the observables, such as the differential branching ratio, the normalized longitudinal polarization fraction $\langle F_L \rangle$, the normalized forward-backward asymmetry $\langle A_{FB} \rangle$, $\langle P_1 \rangle$, $\langle P_2 \rangle$, $\langle P_4' \rangle$, $\langle P_5' \rangle$, and also LFUV sensitive observables such as the ratio of branching ratio $R_{f_2'}$, $\langle Q_{F_L} \rangle$, $\langle Q_{A_{FB}} \rangle$, $\langle Q_i^{(\prime)} \rangle$ in different q^2 bins for both e and the μ mode. Here, we restrict our analysis to the low dilepton invariant mass region ranging from $q^2 \in [0.045, 6.0]$ GeV^2 that excludes the charmonium contributions. We have considered several q^2 bins with similar bin sizes such as [0.10, 0.98], [1.1, 2.5], [2.5, 4.0], and [4.0, 6.0], as reported by LHCb in the measurements of $B_s \to \phi\mu^+\mu^-$ decays [16,17]. In addition, we include [1.1, 6.0] and [0.045, 6.0] bins. The central values for each observable are obtained by considering the central values of each input parameter. The corresponding 1σ uncertainties are obtained by using the uncertainties associated with input parameters such as the form factors, the CKM matrix elements $|V_{tb}V_{ts}^*|$, and the branching ratio $\mathcal{B}(f_2' \to K^+K^-)$. We notice that the branching ratio for $B_s \to f_2'(1525)(\to K^+K^-)\{\mu^+/e^+\}\{\mu^-/e^-\}$ decays is of the order of $\mathcal{O}(10^{-7})$ in the SM. As expected, in the SM both the e and μ modes show similar behavior for all the observables. Obviously, this is a clear confirmation of the LFU in the SM. To account for the LFU, we expect $\langle Q_{F_L} \rangle$, $\langle Q_{A_{FB}} \rangle$, $\langle Q_i^{(\prime)} \rangle$ s ($i \in 1, 2, 4, 5$) to be almost zero, although a slight nonzero contribution may occur due to the difference in the masses of e and μ. In addition, we expect the ratio of branching ratio $R_{f_2'}$ to be almost equal to unity. These are observed to be true from the entries reported in Table VII. In addition to the bins reported for the branching ratio in Table VII, for completeness we also report the branching ratios for μ and e modes in the full q^2 range to be $2.13 \pm 0.43 \times 10^{-7}$ and $2.49 \pm 0.44 \times 10^{-7}$, respectively (excluding the branching ratio of f_2' decay into K^+K^-, explicitly), and these values are found to agree with [41].

We show in Fig. 1 the q^2 distribution of various observables in the low dilepton invariant mass region $q^2 \in [0.045, 6.0]$ GeV^2. The central line corresponds to the central values of each input parameter, whereas to obtain the uncertainty band, we employ a naive χ^2 test on the input parameters. We define χ^2 as

$$\chi^2 = \sum_i \frac{(\mathcal{O}_i - \mathcal{O}_i^C)^2}{\Delta_i^2}, \tag{26}$$

TABLE V. The central values and the corresponding 1σ uncertainties for each of the observables such as the branching ratio, the normalized longitudinal polarization fraction $\langle F_L \rangle$, and the normalized forward-backward asymmetry $\langle A_{FB} \rangle$ for both the e mode and μ mode of $B_s \to f_2'(1525)(\to K^+K^-)l^+l^-$ decays.

	BR $\times 10^{-7}$		$\langle F_L \rangle$		$\langle A_{FB} \rangle$	
q^2 bins (GeV^2)	e mode	μ mode	e mode	μ mode	e mode	μ mode
[0.10, 0.98]	0.116 ± 0.021	0.114 ± 0.021	0.502 ± 0.108	0.503 ± 0.108	0.096 ± 0.017	0.086 ± 0.016
[1.1, 2.5]	0.105 ± 0.025	0.105 ± 0.025	0.854 ± 0.043	0.855 ± 0.047	0.082 ± 0.034	0.082 ± 0.036
[2.5, 4.0]	0.111 ± 0.026	0.110 ± 0.026	0.841 ± 0.045	0.843 ± 0.045	-0.014 ± 0.040	-0.014 ± 0.039
[4.0, 6.0]	0.154 ± 0.035	0.153 ± 0.035	0.760 ± 0.062	0.762 ± 0.062	-0.116 ± 0.050	-0.116 ± 0.049
[1.1, 6.0]	0.370 ± 0.085	0.368 ± 0.085	0.810 ± 0.050	0.812 ± 0.050	-0.029 ± 0.040	-0.030 ± 0.040
[0.045, 6.0]	0.524 ± 0.103	0.512 ± 0.103	0.700 ± 0.071	0.712 ± 0.069	0.004 ± 0.030	-0.000 ± 0.030

TABLE VI. The central values and the corresponding 1σ uncertainties of various angular observables such as $\langle P_1\rangle$, $\langle P_2\rangle$, $\langle P_4'\rangle$, $\langle P_5'\rangle$ for both the e mode and μ mode of $B_s \to f_2'(1525)(\to K^+K^-)l^+l^-$ decays.

	$\langle P_1\rangle$		$\langle P_2\rangle$		$\langle P_4'\rangle$		$\langle P_5'\rangle$	
q^2 bins (GeV^2)	e mode	μ mode	e mode	μ mode	e mode	μ mode	e mode	μ mode
[0.10, 0.98]	-0.008 ± 0.265	-0.008 ± 0.267	0.132 ± 0.024	0.158 ± 0.029	-0.468 ± 0.086	-0.457 ± 0.089	0.554 ± 0.103	0.593 ± 0.114
[1.1, 2.5]	-0.043 ± 0.197	-0.043 ± 0.197	0.373 ± 0.080	0.378 ± 0.081	0.248 ± 0.234	0.251 ± 0.234	-0.076 ± 0.263	-0.079 ± 0.267
[2.5, 4.0]	-0.112 ± 0.240	-0.112 ± 0.240	-0.046 ± 0.157	-0.046 ± 0.158	0.810 ± 0.197	0.811 ± 0.197	-0.616 ± 0.235	-0.620 ± 0.236
[4.0, 6.0]	-0.159 ± 0.282	-0.159 ± 0.282	-0.314 ± 0.081	-0.315 ± 0.082	0.995 ± 0.156	0.995 ± 0.156	-0.794 ± 0.186	-0.797 ± 0.187
[1.1, 6.0]	-0.120 ± 0.221	-0.121 ± 0.222	-0.095 ± 0.128	-0.098 ± 0.128	0.735 ± 0.188	0.739 ± 0.188	-0.546 ± 0.219	-0.552 ± 0.220
[0.045, 6.0]	-0.060 ± 0.179	-0.074 ± 0.175	0.004 ± 0.067	-0.003 ± 0.085	0.307 ± 0.171	0.405 ± 0.183	-0.167 ± 0.185	-0.238 ± 0.204

TABLE VII. The central values and the corresponding 1σ uncertainties of various LFUV sensitive observables, such as the ratio of branching ratio $\langle R_{f_2'}\rangle$, $\langle Q_i^{(\prime)}\rangle$, $\langle Q_{F_L}\rangle$, $\langle Q_{A_{FB}}\rangle$ for $B_s \to f_2'(1525)(\to K^+K^-)l^+l^-$ decays.

q^2 bins (GeV^2)	$\langle R\rangle$	$\langle Q_1\rangle$	$\langle Q_2\rangle$	$\langle Q_4'\rangle$	$\langle Q_5'\rangle$	$\langle Q_{A_{FB}}\rangle$	$\langle Q_{F_L}\rangle$
[0.10, 0.98]	0.979 ± 0.005	0.000 ± 0.003	0.026 ± 0.005	0.011 ± 0.005	0.039 ± 0.011	-0.010 ± 0.002	0.001 ± 0.001
[1.1, 2.5]	0.994 ± 0.005	-0.000 ± 0.001	0.005 ± 0.002	0.002 ± 0.001	-0.002 ± 0.004	-0.002 ± 0.001	0.002 ± 0.001
[2.5, 4.0]	0.995 ± 0.005	-0.000 ± 0.000	-0.001 ± 0.001	0.000 ± 0.000	-0.004 ± 0.002	0.000 ± 0.001	0.002 ± 0.001
[4.0, 6.0]	0.996 ± 0.003	-0.000 ± 0.000	-0.001 ± 0.001	0.000 ± 0.000	-0.004 ± 0.001	0.001 ± 0.000	0.002 ± 0.000
[1.1, 6.0]	0.995 ± 0.002	-0.001 ± 0.002	-0.003 ± 0.001	0.004 ± 0.001	-0.007 ± 0.002	-0.000 ± 0.001	0.002 ± 0.001
[0.045, 6.0]	0.976 ± 0.005	-0.014 ± 0.040	-0.007 ± 0.019	0.098 ± 0.015	-0.071 ± 0.021	-0.004 ± 0.001	0.012 ± 0.002

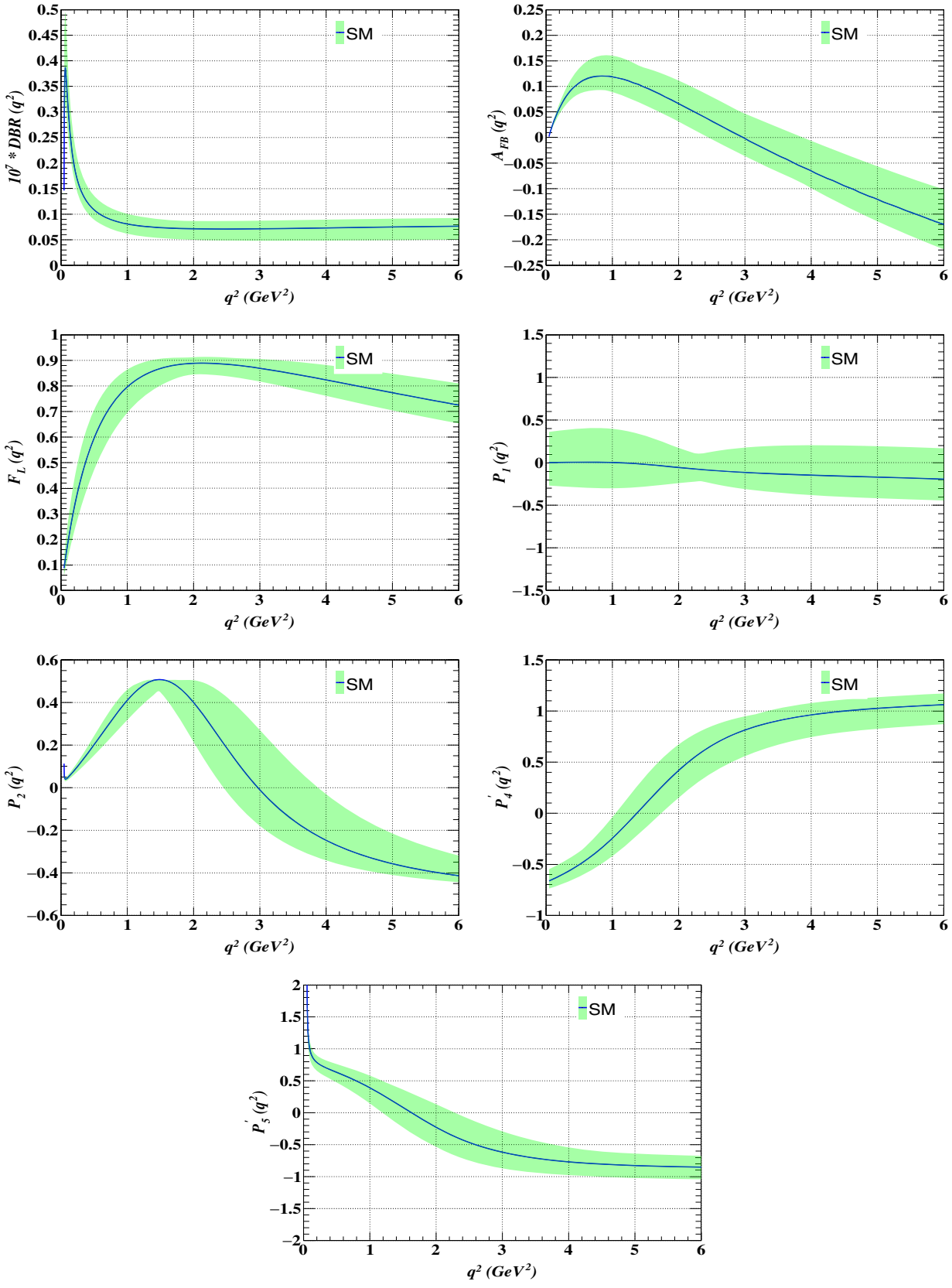

FIG. 1. The q^2 distribution of various observables for the $B_s \to f_2'(1525)(\to K^+K^-)\mu^+\mu^-$ decays in the SM. The band corresponds to the uncertainties in the input parameters such as the $B_s \to f_2'$ transition form factors, the CKM matrix element, and $\mathcal{B}(f_2' \to K^+K^-)$.

TABLE VIII. Best fit values of NP Wilson coefficients [37].

Wilson coefficients	$C_9^{\rm NP}$	$C_{10}^{\rm NP}$	$C_9^{\rm NP}=-C_{10}^{\rm NP}$	$C_9^{\rm NP}=-C_9'$	$(C_9^{\rm NP}, C_{10}^{\rm NP})$	$(C_9^{\rm NP}=-C_9')$	$(C_9^{\rm NP}=-C_{10}')$
Best fit values	−1.07	+0.78	−0.52	−1.11	(−0.94, +0.23)	(−1.27, +0.68)	(−1.36, −0.46)

where $\mathcal{O}_i \in (F(0), a, b, |V_{tb}V_{ts}^*|, \mathcal{B}(f_2' \to K^+K^-))$ and $\mathcal{O}_i^C$ represent the central values of each input parameter. Here Δ_i represents the respective uncertainties associated with each input parameter. To obtain the uncertainty in each observable, we impose $\chi^2 \leq 7.43$ as a constraint. It is important to note that we observe zero crossing in the q^2 distribution of $A_{FB}(q^2)$, $P_2(q^2)$, $P_4'(q^2)$, and $P_5'(q^2)$. Interestingly, the $A_{FB}(q^2)$ and $P_2(q^2)$ have the same zero crossing points, i.e., at $q^2 \sim 3^{+0.8}_{-0.6}$ GeV^2. Similarly, the $P_4'(q^2)$ and $P_5'(q^2)$ have the zero crossing points at around $q^2 \sim 1.4 \pm 0.3$ GeV^2 and $q^2 \sim 1.6 \pm 0.4$ GeV^2, respectively. The value of $P_1(q^2)$ is almost zero in the low q^2 region and becomes negative at higher q^2 regions. The uncertainties associated with $P_i^{(\prime)}(q^2)$ observables are more compared to DBR(q^2), $F_L(q^2)$, and $A_{FB}(q^2)$. The ratio of branching ratio $R_{f_2'}(q^2)$ is almost equal to ∼1 in the whole q^2 region and the uncertainty associated with $R_{f_2'}(q^2)$ is quite negligible in comparison to the uncertainties present in other observables.

C. New physics

In order to explain the anomalies present in $b \to s l^+ l^-$ transition decays, various global fits have been performed by several groups [48–57]. In principle, the NP can enter the effective Hamiltonian through several NP Lorentz structures such as vector, axial vector, scalar, pseudoscalar, and tensor operators. But few measurements, particularly $B_s \to \mu^+\mu^-$ and $b \to s\gamma$, put severe constraint on the scalar, pseudoscalar, and tensor NP Lorentz structures [34–36], and hence they are omitted from our analysis. We refer to Ref. [37] for the global fit results that are performed on the new Wilson coefficients by considering $C_{9,10}^{\rm NP}$ and $C_{9,10}'$. In particular, these NP operators have V-A structure. The authors perform a global fit to these Wilson coefficients by using the constraints coming from observables such as R_K, R_{K^*}, P_5', and $\mathcal{B}(B_s \to \phi\mu^+\mu^-)$. In addition, the fits also include the constraints coming from the branching ratio of $B_s \to \mu^+\mu^-$, the differential branching ratio of $B^0 \to K^{0*}\mu^+\mu^-$, $B^+ \to K^{+*}\mu^+\mu^-$, $B^0 \to K^0\mu^+\mu^-$, $B^+ \to K^+\mu^+\mu^-$, and $B \to X_s\mu^+\mu^-$ in several q^2 bins, and also the constraints from the angular observables in $B^0 \to K^{0*}\mu^+\mu^-$ and $B_s^0 \to \phi\mu^+\mu^-$ decays in several q^2 bins. All the omitted details can be found in Ref. [37]. Out of various 1D and 2D scenarios, we consider seven total NP scenarios that have high $\Delta\chi^2$ values: four from 1D scenarios and three from 2D scenarios. We give bin wise predictions, as well as the q^2 distributions of various observables, and make a comparative study among different NP scenarios and the SM for the $B_s \to f_2'(1525)(\to K^+K^-)l^+l^-$ decay mode. The best fit values of the NP Wilson coefficients pertinent for our analysis and taken from Ref. [37] are reported in Table VIII.

1. New physics: 1D scenario

Let us now discuss the four 1D NP scenarios that arise due to contributions coming from $C_9^{\rm NP}$, $C_{10}^{\rm NP}$, $C_9^{\rm NP}=-C_{10}^{\rm NP}$, and $C_9^{\rm NP}=-C_9'$. The $C_{9,10}^{\rm NP}$ new Wilson coefficients are associated with similar interactions as that of $C_{9,10}$ SM Wilson coefficients, whereas the $C_{9,10}'$ new Wilson coefficients arise due to the right chiral currents which are basically absent in the SM. We report in the Appendix that in Tables IX–XV the average values of various observables such as the BR, $\langle F_L\rangle$, $\langle A_{FB}\rangle$, $\langle P_1\rangle$, $\langle P_2\rangle$, $\langle P_4'\rangle$, $\langle P_5'\rangle$ for the μ mode in several q^2 bins. The corresponding bin wise plots have been displayed in Fig. 2. Our observations are as follows:

(i) BR: In the first bin [0.045, 0.98], although the central values of all the NP scenarios differ slightly from the SM, they all lie within the SM 1σ error band. In the bins [1.1, 2.5], [2.5, 4.0], and [4.0, 6.0], although the central values differ from the SM prediction, no significant deviations are observed, whereas the central value obtained in the case of the $C_9^{\rm NP}=-C_9'$ NP scenario deviates by $1-1.3\sigma$ from the SM expectations. This is true for the larger bin, [1.1, 6.0], as well.

(ii) F_L: In the bin [0.045, 0.98], a deviation of around 1σ from the SM prediction is observed for the $C_9^{\rm NP}=-C_9'$ NP scenario. For the rest of the NP scenarios, the deviation is quite negligible. In the bin [1.1, 2.5], a deviation of around 1.3σ and 2.2σ from the SM prediction is observed in the case of $C_9^{\rm NP}$ and $C_9^{\rm NP}=-C_9'$ NP scenarios, respectively. Similarly, in the bin [2.5, 4.0], the $C_9^{\rm NP}=-C_9'$ NP scenario shows a deviation of around 1.5σ from the SM prediction. Moreover, in the bin [1.0, 6.0], a deviation of around 1.5σ from the SM prediction is observed in the case of $C_9^{\rm NP}=-C_9'$ NP scenario.

(iii) A_{FB}: In the bin [0.045, 0.98], the value of A_{FB} obtained in the case of the $C_9^{\rm NP}=-C_9'$ NP scenario lies outside the SM 1σ error band, whereas, for rest of the NP scenarios, it seems to lie within the SM 1σ error band. In the bin [1.1, 2.5], the $C_{10}^{\rm NP}$ is exactly

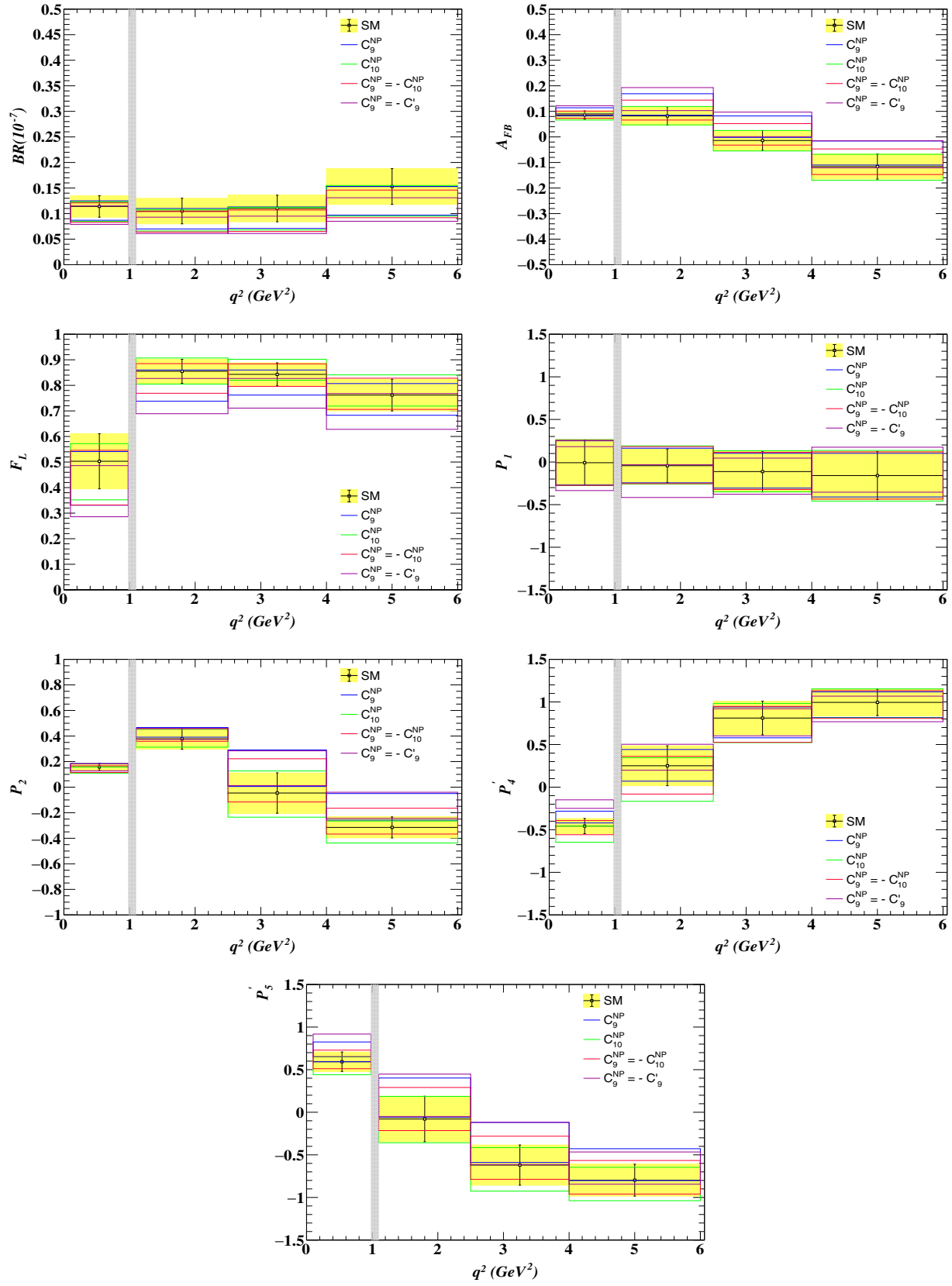

FIG. 2. The central values and the corresponding 1σ error bands of various observables such as the branching ratio, the longitudinal polarization fraction F_L, the forward-backward asymmetry A_{FB}, and P_1, P_2, P_4', P_5' for the $B_s \to f_2'(1525)(\to K^+K^-)\mu^+\mu^-$ decays in several q^2 bins in the SM and in the presence of four 1D NP scenarios.

like the SM, whereas, $C_9^{\rm NP}$ and $C_9^{\rm NP} = -C_9'$ show around 1.5σ and 2σ deviation from the SM prediction. In the bin [2.5, 4.0], a deviation of around 1.4σ and 1.6σ is observed in case of $C_9^{\rm NP}$ and $C_9^{\rm NP} = -C_9'$ NP scenarios, whereas, in the case of $C_{10}^{\rm NP}$, it is exactly like the SM.

(iv) P_1: Although the central values of P_1 obtained in each NP scenario differs from the SM central value, they lie within the SM 1σ error band and hence can not be distinguished from the SM predictions.

(v) P_2: No significant deviations from the SM prediction are observed in the first two bins, i.e., in [0.045, 0.98] and [1.1, 2.5]. However, in bins [2.5, 4.0] and [4.0, 6.0], the deviations observed in the case of the $C_9^{\rm NP}$ and $C_9^{\rm NP} = -C_9'$ NP scenarios are distinguishable from the SM prediction at the level of 1.3σ and 2σ significance.

(vi) P_4': Although there is slight deviation in case of $C_9^{\rm NP}$ and $C_{10}^{\rm NP}$ NP scenarios, they lie within the SM 1σ error band in almost all q^2 bins. Similarly, with $C_9^{\rm NP} = -C_{10}^{\rm NP}$, it is exactly SM-like. With the $C_9^{\rm NP} = -C_9'$ NP scenario, we observe a deviation of around 2.5σ from the SM expectations in [0.045, 0.98] bin which is clearly distinguishable from the SM prediction.

(vii) P_5': No significant deviation from the SM prediction is observed. The only exception is $C_9^{\rm NP} = -C_9'$ NP scenario in which a deviation of around 1σ from the SM prediction is observed in the $q^2 \in [0.045, 0.98]$ bin. It should be noted that the value of P_5' obtained with the rest of the NP couplings lies within the SM error band.

We show in Fig. 3 the q^2 dependent observables for the $B_s \to f_2'(1525)\mu^+\mu^-$ decays in the presence of several NP WCs in the 1D scenario. The SM error band is shown with green. The detailed observations are as follows:

(i) The differential branching ratio $\mathrm{DBR}(q^2)$ is slightly reduced at all q^2 for each NP scenario and it lies within the SM 1σ error band.

(ii) It is interesting to note that the zero crossing point of $A_{FB}(q^2)$ is shifted towards the higher q^2 regions than in the SM for most of the NP scenarios. However, it coincides with the SM zero crossing point $q^2 \sim 3^{+0.8}_{-0.6}$ GeV^2 for $C_{10}^{\rm NP}$ NP coupling. We observe the zero crossing of $A_{FB}(q^2)$ at $q^2 \sim 3.3$ GeV^2 for the $C_9^{\rm NP} = -C_{10}^{\rm NP}$ scenario. Similarly, the zero crossing is observed at around $q^2 \sim 3.8$ GeV^2 for $C_9^{\rm NP}$ and $C_9^{\rm NP} = -C_9'$ NP scenarios, respectively. It is worth mentioning that the zero crossing points for $C_9^{\rm NP}$ and $C_9^{\rm NP} = -C_9'$ NP scenarios are distinguishable from the SM prediction at the level of 1σ significance.

(iii) For the longitudinal polarization fraction $F_L(q^2)$, the q^2 distribution obtained for $C_{10}^{\rm NP}$ and $C_9^{\rm NP} = -C_{10}^{\rm NP}$ NP scenarios is quite similar to that of the SM. In the case of $C_9^{\rm NP}$, it lies outside the SM error band in the $q^2 \in [1.1, 2.5]$ region and becomes very similar to the SM curve in the higher q^2 regions. The maximum deviation from the SM prediction is observed for the $C_9^{\rm NP} = -C_9'$ NP scenario.

(iv) For the angular observable $P_1(q^2)$, the q^2 distribution obtained for $C_9^{\rm NP}$, $C_{10}^{\rm NP}$, and $C_9^{\rm NP} = -C_{10}^{\rm NP}$ NP scenarios is quite similar to the SM. The shape, however, is different from the SM in the case of the $C_9^{\rm NP} = -C_9'$ NP scenario. The value of $P_1(q^2)$ obtained in this NP scenario is negative in the whole q^2 region and reaches its minimum of around -0.25 at $q^2 = 2$ GeV^2.

(v) In the case of $P_2(q^2)$, similar to $A_{FB}(q^2)$, the zero crossing point is shifted towards the higher q^2 regions than in the SM for most of the NP scenarios. The maximum deviation in the zero crossing point is observed in the case of $C_9^{\rm NP}$ and $C_9^{\rm NP} = -C_9'$ NP scenarios, respectively.

(vi) The angular observable $P_4'(q^2)$ obtained in each of these $1D$ scenarios lies within the SM error band. There is, however, one exception. For $C_9^{\rm NP} = -C_9'$, it lies outside the SM 1σ error band in the low q^2 region, i.e., for $q^2 \leq 1$ GeV^2. In addition, the zero crossing points for the $C_9^{\rm NP} = -C_{10}^{\rm NP}$ and $C_{10}^{\rm NP}$ NP scenarios are observed at $q^2 \sim 1.5$ GeV^2 and $q^2 \sim 1.6$ GeV^2, whereas, the zero crossing points for $C_9^{\rm NP}$ and $C_9^{\rm NP} = -C_9'$ are observed at $q^2 \sim 1.3$ GeV^2 and $q^2 \sim 1$ GeV^2, respectively. It is worth mentioning that the zero crossing point obtained in the case of the $C_9^{\rm NP} = -C_9'$ NP scenario is distinguishable from the SM zero crossing point $q^2 \sim 1.4 \pm 0.3$ GeV^2 at more than 1σ significance.

(vii) For the angular observable $P_5'(q^2)$, the zero crossing point obtained in each NP scenario is shifted towards the higher value of q^2 than in the SM except for $C_{10}^{\rm NP}$. In the case of $C_{10}^{\rm NP}$, the zero crossing point coincides with the SM zero crossing point of $q^2 \sim 1.6 \pm 0.4$ GeV^2. For $C_9^{\rm NP} = -C_{10}^{\rm NP}$ NP scenario, the zero crossing point is observed at $q^2 \sim 1.8$ GeV^2, whereas for $C_9^{\rm NP}$ and $C_9^{\rm NP} = -C_9'$ NP scenarios, we observe the zero crossing point at $q^2 \sim 2.1$ GeV^2 which deviates from the SM prediction at the level of around 1σ significance.

2. New physics: 2D scenario

Now we proceed to discuss the impact of several new Wilson coefficients from the $2D$ scenarios. We consider

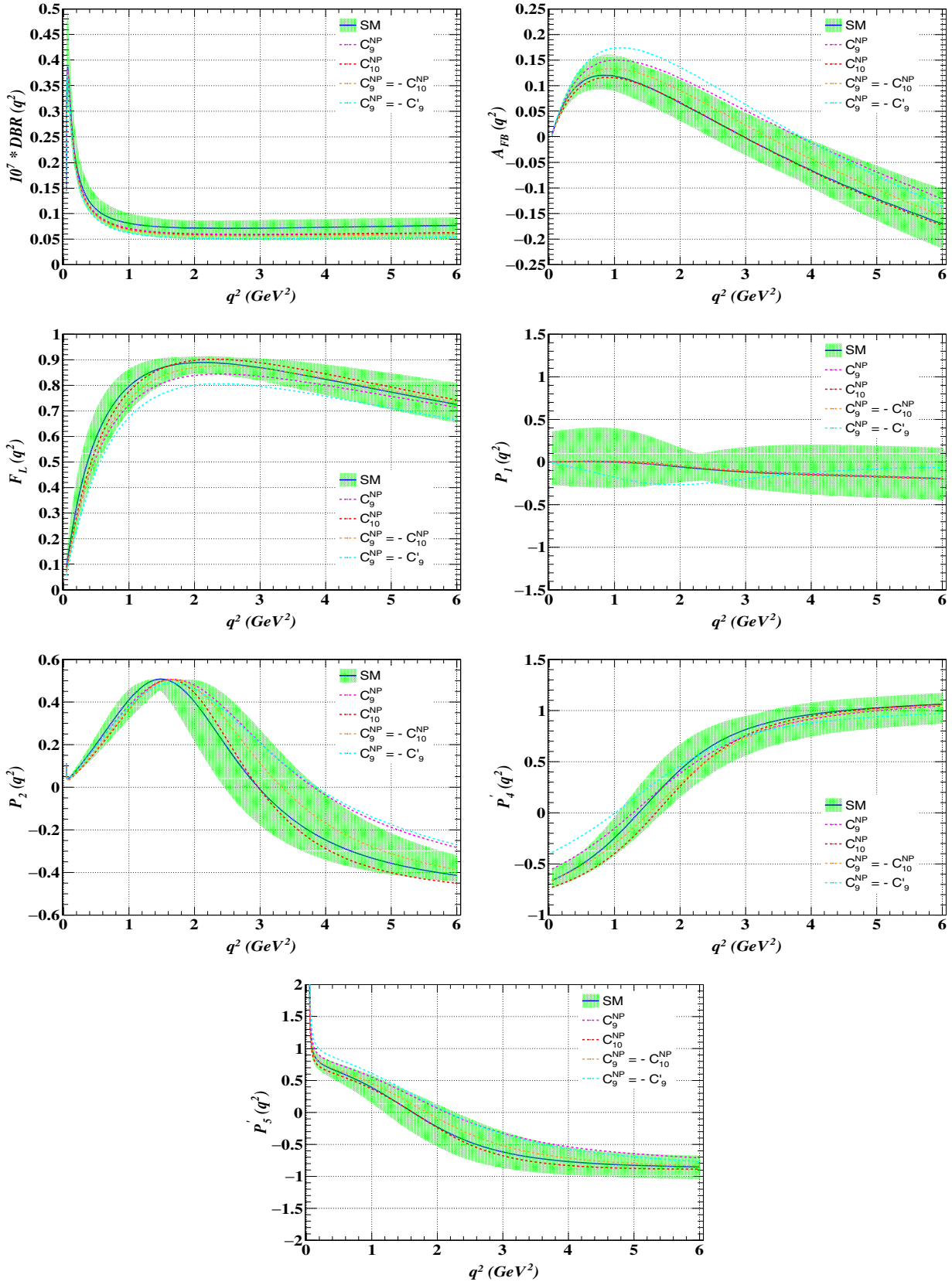

FIG. 3. The q^2 distributions of various observables such as the differential branching ratio DBR(q^2), the longitudinal polarization fraction $F_L(q^2)$, the forward-backward asymmetry $A_{FB}(q^2)$, and $P_1(q^2)$, $P_2(q^2)$, $P_4'(q^2)$, $P_5'(q^2)$ for the $B_s \to f_2'(1525)(\to K^+K^-)\mu^+\mu^-$ decays in the SM and in the presence of $C_9^{\rm NP}$, $C_{10}^{\rm NP}$, $C_9^{\rm NP} = -C_{10}^{\rm NP}$ and $C_9^{\rm NP} = -C_9'$ 1D NP scenarios.

three different 2D scenarios: $(C_9^{\rm NP}, C_{10}^{\rm NP})$, $(C_9^{\rm NP}, C_9')$, and $(C_9^{\rm NP}, C_{10}')$. We report in the Appendix the average values of all the observables for the μ mode in the Tables IX–XV. Similarly, the bin wise q^2 distribution plots are shown in Fig. 4. The discussions pertaining to the impact of 2D new WCs on various observables are as follows:

(i) BR: Although the central values obtained for each NP scenario differ from the SM prediction, and no significant deviation is observed in any q^2 bins. The deviation from the SM prediction is observed to be around 1σ in the case of $(C_9^{\rm NP}, C_9')$ and $(C_9^{\rm NP}, C_{10}')$ NP scenarios, whereas, for the $(C_9^{\rm NP}, C_{10}^{\rm NP})$ NP scenario, the value of BR lies within the SM 1σ error band.

(ii) F_L: In the bin $q^2 \in [1.1, 2.5]$, a deviation of around 1.1σ from the SM prediction is observed in the case of $(C_9^{\rm NP}, C_9')$ and $(C_9^{\rm NP}, C_{10}')$ NP scenarios. In all other q^2 bins, the value of F_L lies within the 1σ SM error band for each NP scenario.

(iii) A_{FB}: In the bin $q^2 \in [1.1, 2.5]$ and $q^2 \in [2.5, 4.0]$, the deviation from the SM prediction is observed to be at the $1.1 - 1.2\sigma$ level in the case of $(C_9^{\rm NP}, C_9')$ and $(C_9^{\rm NP}, C_{10}')$ NP scenarios. In all other bins, it lies within the SM 1σ error band for each NP scenario.

(iv) P_1: Although the central values obtained for each NP scenario differ from the SM central values, no significant deviation is observed as they all lie within the SM 1σ error band.

(v) P_2: A deviation of around $1 - 1.1\sigma$ from the SM prediction is observed in the bin $q^2 \in [2.5, 4.0]$ in the case of $(C_9^{\rm NP}, C_9')$ and $(C_9^{\rm NP}, C_{10}')$ NP scenarios. Similarly, in the $q^2 \in [4.0, 6.0]$ bin, a deviation of around 1.5σ is observed in the case of $(C_9^{\rm NP}, C_9')$ and $(C_9^{\rm NP}, C_{10}')$ NP scenarios.

(vi) P_4': In the bin $q^2 \in [0.045, 0.98]$, the $(C_9^{\rm NP}, C_9')$ NP scenario is distinguishable from the SM prediction at the level of 2σ significance, whereas, in case of $(C_9^{\rm NP}, C_{10}^{\rm NP})$ and $(C_9^{\rm NP}, C_{10}')$ NP scenarios, the value of P_4' lies within the SM 1σ error band and hence can not be distinguished from the SM prediction.

(vii) P_5': In the bin $q^2 \in [0.045, 0.98]$, the value of P_5' obtained in the case of the $(C_9^{\rm NP}, C_9')$ NP scenario shows a deviation of around 1σ from the SM prediction, whereas, with other NP scenarios, it is consistent with the SM prediction. Similarly, in the bins $q^2 \in [1.1, 2.5]$, [2.5, 4.0], and [4.0, 6.0], no significant deviation from the SM prediction is observed and they are indistinguishable from the SM.

We show in Fig. 5 the q^2 dependence of all the observables for the $B_s \to f_2'(1525)\mu^+\mu^-$ decays in several $2D$ scenarios. The SM 1σ error band is shown with green. The detailed observations are as follows:

(i) Similar to the $1D$ scenario, we observe that the differential branching ratio is slightly reduced at all q^2 for each NP scenario and they all lie within the SM error band.

(ii) It is worth mentioning that the zero crossing point for $A_{FB}(q^2)$ is shifted to a higher q^2 region for all the NP scenarios as compared to the SM. The zero crossing points for $A_{FB}(q^2)$ are observed at $q^2 \sim 3.6$ GeV^2, $q^2 \sim 4$ GeV^2, and $q^2 \sim 4.1$ GeV^2 for $(C_9^{\rm NP}, C_{10}^{\rm NP})$, $(C_9^{\rm NP}, C_9')$, and for $(C_9^{\rm NP}, C_{10}')$ NP scenarios, respectively. Although all the values are found to be distinct from the SM zero crossing point, it is important to note that the zero crossing point obtained in the case of $(C_9^{\rm NP}, C_9')$ and $(C_9^{\rm NP}, C_{10}')$ NP scenarios are distinguishable from the SM prediction at the level of more than 1σ significance.

(iii) The peak of the longitudinal polarization fraction $F_L(q^2)$ may shift towards higher q^2 values than in the SM for each NP scenarios. It should be mentioned that the peak of $F_L(q^2)$ obtained in the case of $(C_9^{\rm NP}, C_9')$ and $(C_9^{\rm NP}, C_{10}')$ is distinguishable from the SM prediction at a level of more than 1σ significance.

(iv) The angular observable $P_1(q^2)$ is zero in the SM in the low q^2 region, i.e., for $q^2 \leq 1.2$ GeV^2, and becomes negative as q^2 increases. Similar behavior is observed in the case of the $(C_9^{\rm NP}, C_{10}^{\rm NP})$ NP scenario as well. For the $(C_9^{\rm NP}, C_9')$ NP scenario, it deviates slightly away from the SM and reaches a minimum value of around -0.2 at $q^2 = 2$ GeV^2. However, we observe a completely different behavior in the case of the $(C_9^{\rm NP}, C_{10}')$ NP scenario. The value of $P_1(q^2)$ acquires positive values in the whole q^2 region and reaches its maximum value of 0.1 at $q^2 \sim 2.2$ GeV^2. Since the SM error band is too large, the q^2 distributions of all the NP scenarios lie within the SM error band.

(v) The peak of $P_2(q^2)$ is slightly reduced and shifted towards the higher q^2 values in each NP scenarios as compared to the SM. Moreover, the zero crossing point is also shifted to higher values of q^2 than in the SM for all the NP scenarios. In the case of $(C_9^{\rm NP}, C_9')$ and $(C_9^{\rm NP}, C_{10}')$ NP scenarios, the zero crossing points are distinguishable from the SM zero crossing at the a level of more than 1σ significance.

(vi) For the angular observable $P_4'(q^2)$, no significant deviation from the SM is observed for each NP scenario. However, in the low q^2 region, i.e., $q^2 \leq 1$ GeV^2, we see significant deviation of $P_4'(q^2)$ from the SM prediction in the case of the $(C_9^{\rm NP}, C_9')$ NP scenario. Similarly, the zero crossing point of $P_4'(q^2)$ obtained in the case of $(C_9^{\rm NP}, C_{10}')$

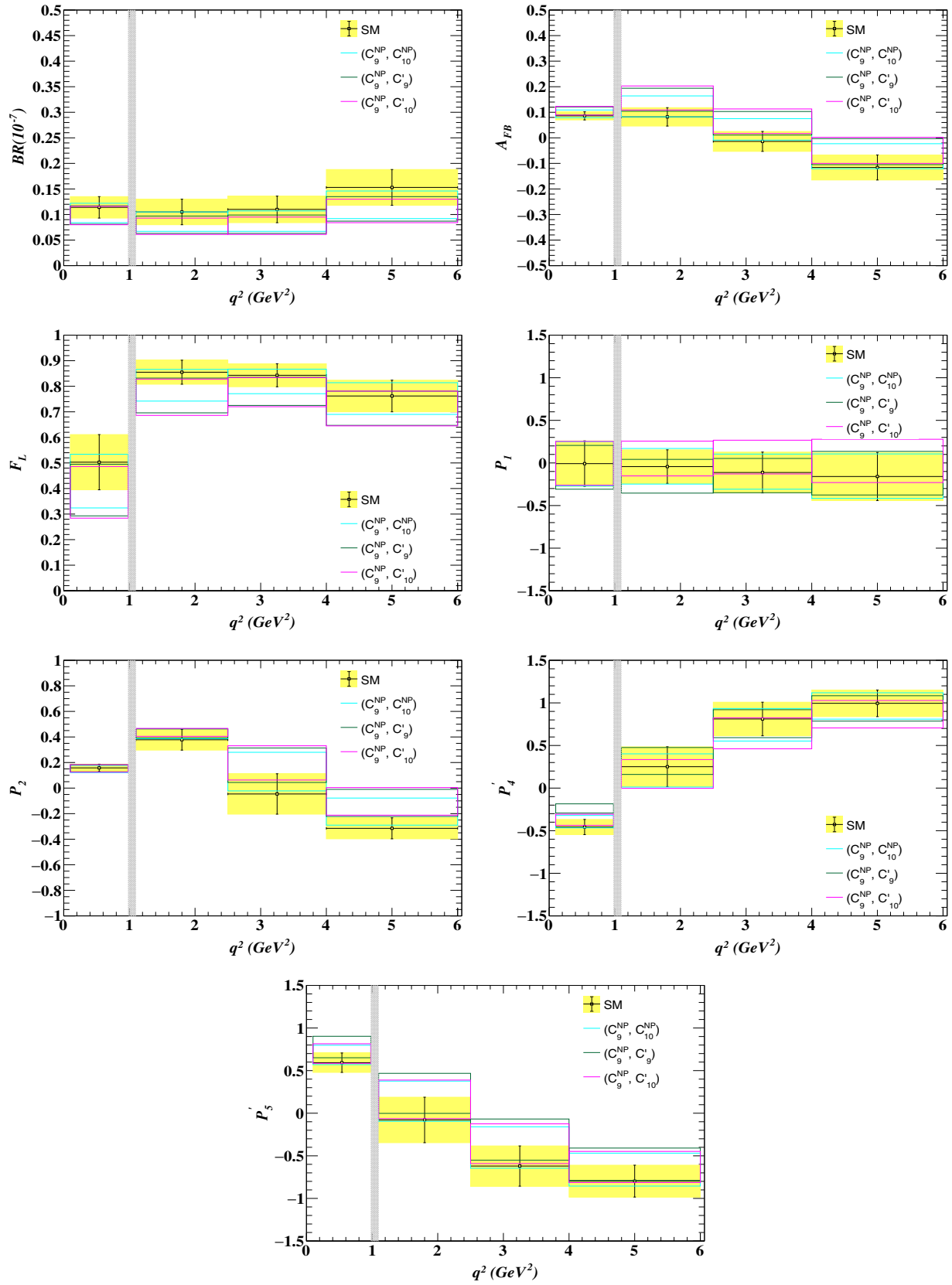

FIG. 4. The central values and the corresponding 1σ error bands of various observables such as the branching ratio, the longitudinal polarization fraction F_L, the forward-backward asymmetry A_{FB}, and P_1, P_2, P_4', P_5' in several q^2 bins for the $B_s \to f_2'(1525)(\to K^+K^-)\mu^+\mu^-$ decays in the SM and in the presence of three 2D NP scenarios.

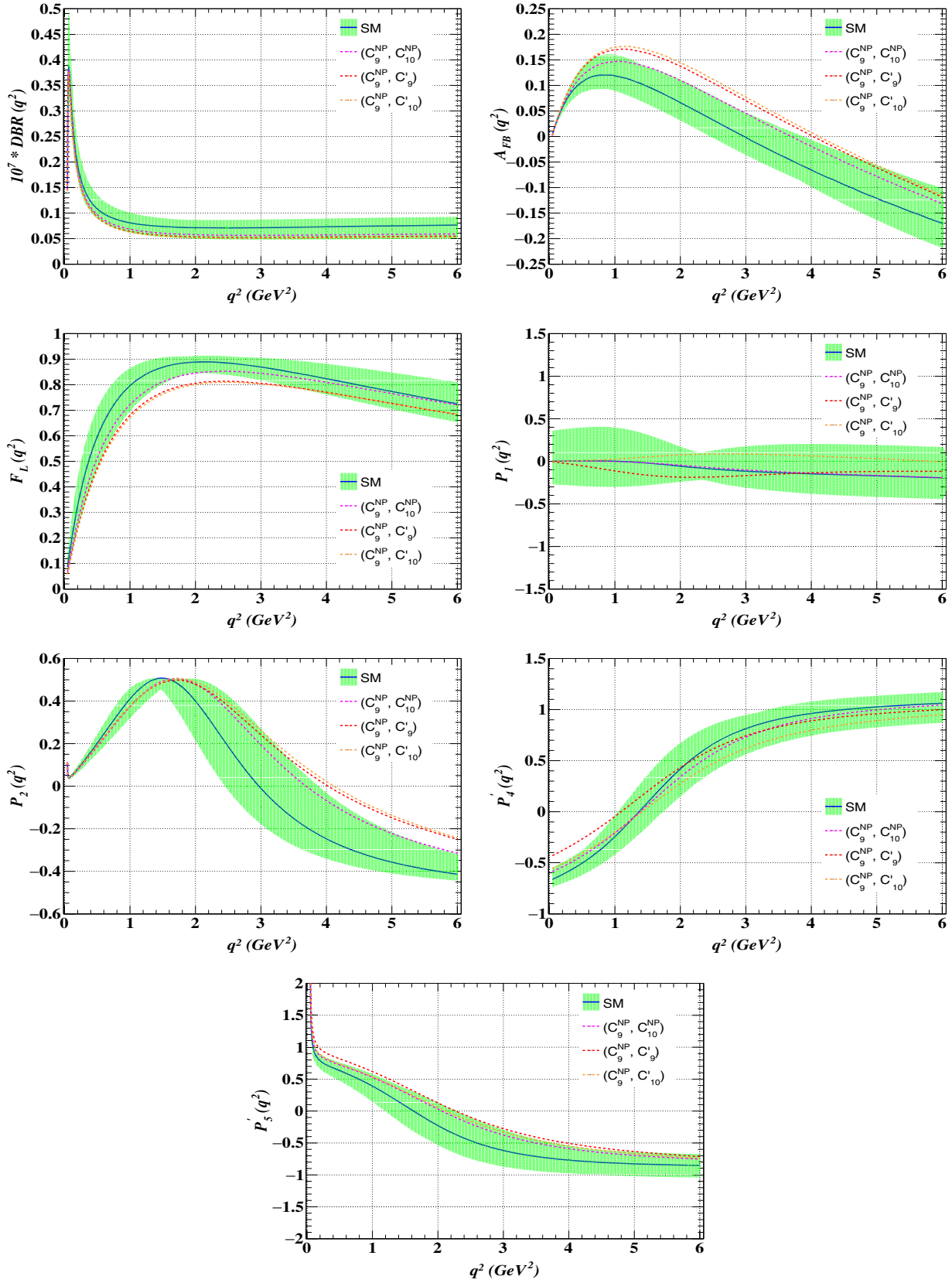

FIG. 5. The q^2 distributions of various observables such as the differential branching ratio DBR(q^2), the longitudinal polarization fraction $F_L(q^2)$, the forward-backward asymmetry $A_{FB}(q^2)$, and $P_1(q^2)$, $P_2(q^2)$, $P_4'(q^2)$, $P_5'(q^2)$ for the $B_s \to f_2'(1525)(\to K^+K^-)\mu^+\mu^-$ decays in the SM, and in the presence of $(C_9^{\rm NP}, C_{10}^{\rm NP})$, $(C_9^{\rm NP}, C_9')$, and $(C_9^{\rm NP}, C_{10}')$ 2D NP scenarios.

and $(C_9^{\rm NP}, C_{10}^{\rm NP})$ NP scenarios coincides with the SM zero crossing point of $q^2 \sim 1.4 \pm 0.3$ GeV^2, whereas, for the $(C_9^{\rm NP}, C_9')$ NP scenario, the zero crossing point is observed at $q^2 \sim 1.1$ GeV^2 and it is distinguishable from the SM zero crossing point at the level of 1σ significance.

(vii) The q^2 distribution of the angular observable $P_5'(q^2)$ obtained in each NP scenario is quite distinct from the SM. The maximum deviation from the SM prediction is observed for the $(C_9^{\rm NP}, C_9')$ NP scenario. The zero crossing points for all the three NP scenarios lie within $q^2 \sim 2.1$–2.3 GeV^2, and interestingly, the zero crossing point for $(C_9^{\rm NP}, C_9')$ is distinguishable from the SM at more than 1.5σ significance.

D. Sensitivity of LFUV observables in $B_s \to f_2'(1525)(\to K^+K^-)\mu^+\mu^-$ decays

The study of LFUV in $B_s \to f_2'(1525)(\to K^+K^-)\mu^+\mu^-$ decays is interesting because it is mediated via similar $b \to s l^+ l^-$ quark level transition, and in principle, it can provide complementary information regarding the anomalies present in $B \to (K, K^*)\mu^+\mu^-$ decay modes. We study the violation of LFU in two different 1D and 2D NP scenarios. We make a comparative study of the LFUV sensitive observables such as $\langle R_{f_2'}\rangle$, $\langle Q_{F_L}\rangle$, $\langle Q_{A_{FB}}\rangle$, and $\langle Q_i^{(\prime)}\rangle$ ($i \in 1, 2, 4, 5$) in the SM and in several 1D and 2D NP scenarios. We report in the Appendix the binned average values of each of the observables in Tables XVI–XXII. Similarly, the bin wise q^2 distribution plots for both $1D$ and $2D$ scenarios are shown in Figs. 6 and 7, respectively. Our observations are as follows:

1. 1D scenario

(i) $R_{f_2'}$: Except in the low q^2 bin, all the NP scenarios are distinguishable from the SM prediction at more than 5σ significance. Hence, a measurement of $R_{f_2'}$ will be crucial to probe NP in $b \to s l^+ l^-$ transition decays.

(ii) Q_1: The value of Q_1 obtained in the case of the $C_9^{\rm NP} = -C_9'$ NP scenario is distinguishable from the SM prediction at the level of $4 - 5\sigma$ significance in the $q^2 \in [0.045, 0.98]$ and $[1.1, 2.5]$ bins. In the rest of the bins, although the central values obtained in each NP scenario differ significantly from the SM, the SM band overlaps with the NP band.

(iii) Q_2: The value of Q_2 obtained in the case of $C_9^{\rm NP}$ and $C_9^{\rm NP} = -C_9'$ NP scenarios are distinguishable from the SM prediction at the level of more than 5σ significance in the region $q^2 \in [2.5, 6.0]$.

(iv) Q_4': In the bin $q^2 \in [1.1, 2.5]$, the $C_{10}^{\rm NP}$ and $C_9^{\rm NP} = -C_{10}^{\rm NP}$ NP scenarios are distinguishable at $5 - 6\sigma$ from the SM. Although, the central values for $C_9^{\rm NP}$ and $C_9^{\rm NP} = -C_9'$ differ significantly from the SM expectations, the associated error band is too large and the SM band overlaps with the NP band. Similarly, for $q^2 \geq 4$ the $C_9^{\rm NP} = -C_9'$ NP scenario is distinguishable at 4.8σ from the SM expectations.

(v) Q_5': In the bin $q^2 \in [1.1, 2.5]$, the value of Q_5' obtained in case of $C_9^{\rm NP}$, $C_9^{\rm NP} = -C_{10}^{\rm NP}$ and $C_9^{\rm NP} = -C_9'$ NP scenarios are clearly distinguishable from the SM prediction at more than 5σ significance. Similarly, the $C_9^{\rm NP}$ and $C_9^{\rm NP} = -C_9'$ NP scenarios are distinguishable at more than 3σ significance from the SM expectations for $q^2 \leq 4$ GeV^2. For $q^2 \geq 4$ GeV^2, the $C_9^{\rm NP}$ and $C_9^{\rm NP} = -C_9'$ NP scenarios are clearly distinguishable from the SM at the level of 4.4σ and 2.5σ significance, respectively.

(vi) $Q_{A_{FB}}$: The value of $Q_{A_{FB}}$ obtained in the case of the $C_9^{\rm NP}$, $C_9^{\rm NP} = -C_{10}^{\rm NP}$ and $C_9^{\rm NP} = -C_9'$ NP scenarios are clearly distinguishable from the SM prediction at the level of more than 3σ significance, whereas, for the $C_{10}^{\rm NP}$ NP scenario, it is SM-like.

(vii) Q_{F_L}: In the low q^2 region, the value of Q_{F_L} deviates significantly from the SM prediction for all the NP scenarios and it is clearly distinguishable from the SM prediction at more than 5σ significance. Similarly, for $q^2 \geq 1$, except for $C_{10}^{\rm NP}$, the $C_9^{\rm NP}$, $C_9^{\rm NP} = -C_{10}^{\rm NP}$ NP scenarios are distinguishable from the SM at the level of 3σ significance.

2. 2D scenario

(i) $R_{f_2'}$: All the NP scenarios are distinguishable at more than 3σ from the SM prediction and in particular, the deviation of $R_{f_2'}$ from the SM prediction in the case of $(C_9^{\rm NP}, C_9')$ and $(C_9^{\rm NP}, C_{10}')$ NP scenarios are quite significant and it is clearly distinguishable from the SM prediction at more than 5σ significance.

(ii) Q_1: The deviation observed in the case of the $(C_9^{\rm NP}, C_{10}')$ NP scenario is clearly distinguishable from the SM prediction at more than 3σ significance in all q^2 bins. Again, for the $(C_9^{\rm NP}, C_9')$ NP Scenario, although the central values differ significantly from the SM, the associated error band is too large in $q^2 \geq 2.5$ bins and the SM value overlaps with the NP band.

(iii) Q_2: No significant deviation is found in $q^2 \leq 2.5$ bins, whereas, for the $q^2 \geq 2.5$ bin, the deviation observed in the case of $(C_9^{\rm NP}, C_9')$ and $(C_9^{\rm NP}, C_{10}')$ is quite significant and it is distinguishable from the SM prediction at more than 5σ significance.

(iv) Q_4': In the low q^2 bin, the deviation observed in the case of $(C_9^{\rm NP}, C_9')$ is clearly distinguishable from the SM prediction. In the $q^2 \in [2.5, 4.0]$ bin, the value of Q_4' obtained in the case of $(C_9^{\rm NP}, C_{10}^{\rm NP})$ is distinguishable from the SM prediction at 3σ significance,

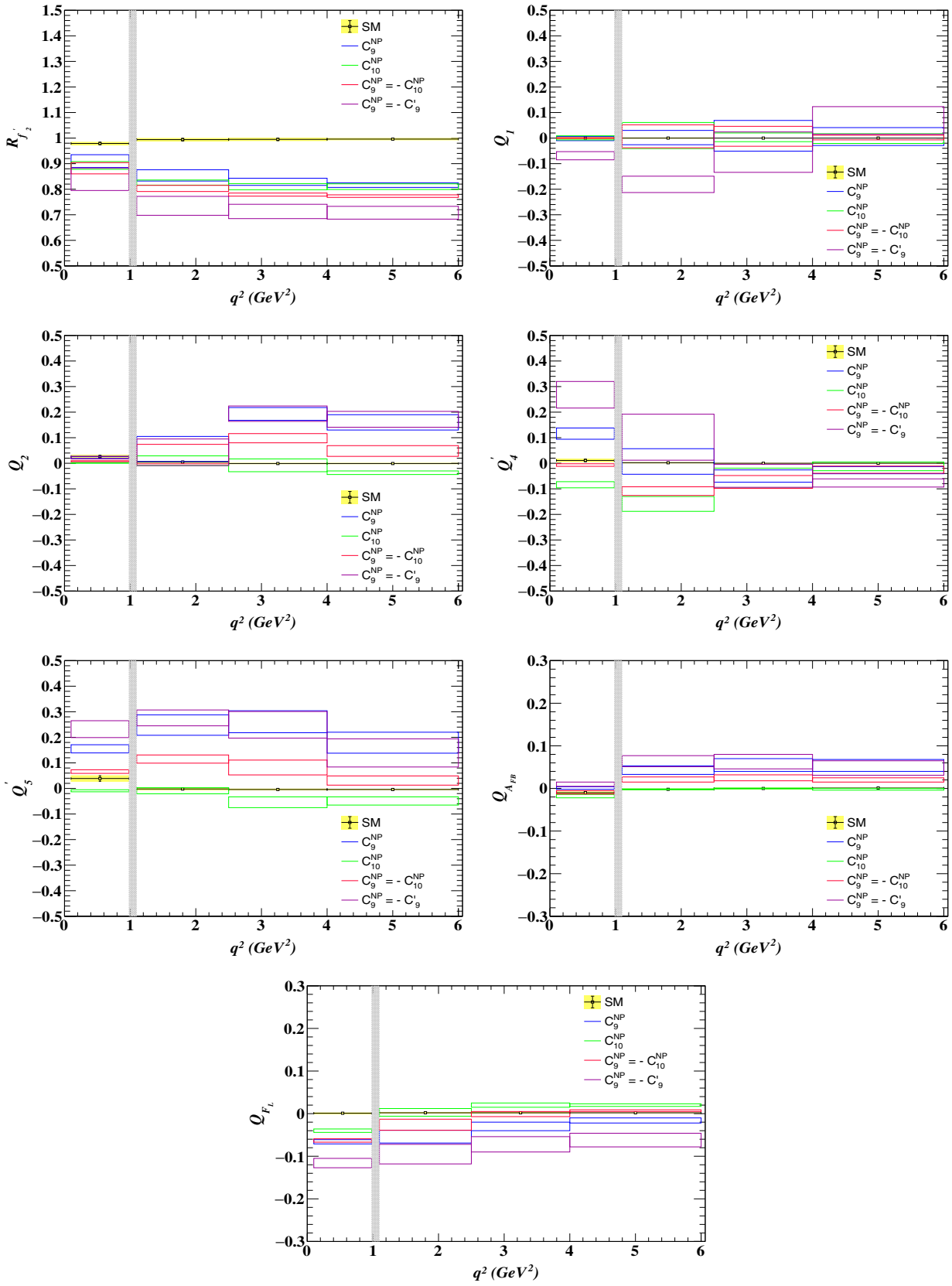

FIG. 6. The central values and the corresponding 1σ error bands of various LFUV sensitive observables such as $\langle R_{f_2'} \rangle$, $\langle Q_i^{(\prime)} \rangle$, $\langle Q_{A_{FB}} \rangle$, and $\langle Q_{F_L} \rangle$ in several q^2 bins in the SM and in the presence of four 1D NP scenarios.

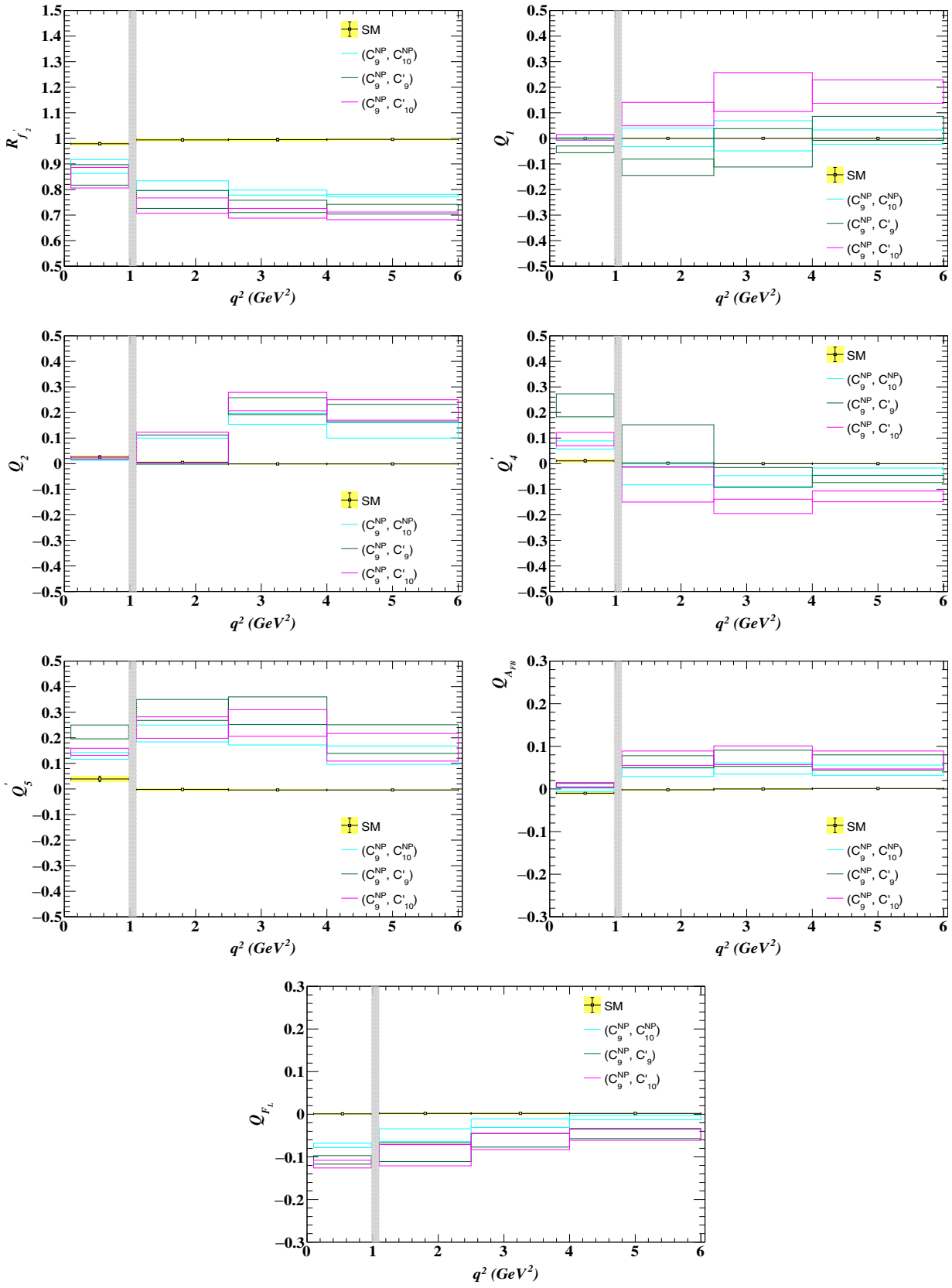

FIG. 7. The central values and the corresponding 1σ error bands of various LFUV sensitive observables such as $\langle R_{f_2'}\rangle$, $\langle Q_i^{(\prime)}\rangle$, $\langle Q_{A_{FB}}\rangle$, and $\langle Q_{F_L}\rangle$ in several q^2 bins in the SM and in the presence of three 2D NP scenarios.

whereas, in the case of the $(C_9^{\rm NP}, C_{10}')$ NP scenario, it is distinguishable at more than 5σ significance. Similarly, in the $q^2 \geq 4$ bin, $(C_9^{\rm NP}, C_9')$ and $(C_9^{\rm NP}, C_{10}')$ NP scenarios are clearly distinguishable from the SM prediction at more than 4σ significance.

(v) Q_5': Although the deviation from the SM prediction is observed to be more pronounced in the case of the $(C_9^{\rm NP}, C_9')$ NP scenario, the value of Q_5' obtained in each NP scenario is clearly distinguishable from the SM prediction at more than 5σ significance.

(vi) $Q_{A_{FB}}$: We observe significant deviation from the SM prediction for each NP scenario. It should be noted that the value of $Q_{A_{FB}}$ obtained in each NP scenario is clearly distinguishable from the SM prediction at more than 3σ significance.

(vii) Q_{F_L}: In the low q^2 bin, all three NP scenarios are clearly distinguishable from the SM at more than 5σ significance. Similarly, for the $q^2 \geq 1$ bins, the value of Q_{F_L} obtained in the case of $(C_9^{\rm NP}, C_9')$ and $(C_9^{\rm NP}, C_{10}')$ NP scenarios is distinguishable from the SM prediction at more than 3σ significance.

IV. CONCLUSION

In light of the recent flavor anomalies reported in $B \to (K, K^*)\mu^+\mu^-$ and $B_s \to \phi\mu^+\mu^-$ decays, we analyze $B_s \to f_2'(1525)\mu^+\mu^-$ decays mediated via similar $b \to sl^+l^-$ neutral current quark level transition. We perform a detailed angular study of the four-body differential decay of $B_s \to f_2'(1525)(\to K^+K^-)\mu^+\mu^-$ within a model independent effective theory formalism. We give predictions of several observables in SM and in the presence of various 1D and 2D NP scenarios proposed in several global fits. In the SM, we obtain the branching ratio of $B_s \to f_2'(1525)(\to K^+K^-)\mu^+\mu^-$ decays to be of the order of $\mathcal{O}(10^{-7})$. We observe that the branching ratio is reduced at all q^2 for most of the NP cases. Except for $C_{10}^{\rm NP}$, in all other NP scenarios the zero crossing point for $A_{FB}(q^2)$ is shifted to the higher q^2 values than in the SM. In the case of F_L, the peak seems to be reduced and shifted to the higher values of q^2 in comparison to the SM. It is worth mentioning that the zero crossing for $A_{FB}(q^2)$ is quite interesting and can, in principle, give useful information regarding lepton flavor universality violation in $b \to sl^+l^-$ transition decays. Importantly, we do observe significant contributions coming from $C_9^{\rm NP} = -C_9'$ in the 1D scenario and $(C_9^{\rm NP}, C_9')$ and $(C_9^{\rm NP}, C_{10}')$ in the 2D scenario. Specially, these primed operators which correspond to right-handed currents seem to be very interesting. As expected, the lepton flavor universal ratio $\langle R_{f_2'} \rangle$, and other Q observables such as $\langle Q_i^{(\prime)} \rangle$, $\langle Q_{A_{FB}} \rangle$, and $\langle Q_{F_L} \rangle$, are exceptionally clean observables with a theoretical uncertainty of only 1%, which makes them ideal candidates to probe NP in $b \to sl^+l^-$ transition decays. Although there have been several hints of NP reported in $b \to sl^+l^-$ transition decays, existence of NP is yet to be confirmed. Unlike $B \to (K, K^*)\mu^+\mu^-$ and $B_s \to \phi\mu^+\mu^-$ decays which have caught more attention from the theorists and experimentalists, the $B_s \to f_2'(1525)(\to K^+K^-)\mu^+\mu^-$ decays mediated via the same quark level transitions have received less attention so far. Measurements of various observables for this decay mode in the future can shed more light on identifying the exact NP Lorentz structures. At the same time, better theoretical understanding of the $B_s \to f_2'$ transition form factors in the future will be crucial to disentangling genuine NP effects from the SM uncertainties. More data samples are also needed in order to enhance the significance of the various measurements and to reduce the statistical and systematic uncertainties to properly disentangle the NP effects.

ACKNOWLEDGMENTS

The author N. S. would like to thank Thomas Blake for several useful discussions.

APPENDIX A: PREDICTIONS OF VARIOUS PHYSICAL OBSERVABLES IN THE SM AND IN THE PRESENCE VARIOUS 1D AND 2D NP COUPLINGS FOR THE $B_s \to f_2'(1525)(\to K^+K^-)\mu^+\mu^-$ DECAYS

TABLE IX. The binned average central values and the corresponding 1σ uncertainties for the branching ratio BR $\times 10^{-7}$ of $B_s \to f_2'(1525)(\to K^+K^-)\mu^+\mu^-$ decays in the SM and in several NP cases.

q^2 bins (GeV^2)	BR $\times 10^{-7}$							
	SM	$C_9^{\rm NP}$	$C_{10}^{\rm NP}$	$C_9^{\rm NP} = -C_{10}^{\rm NP}$	$C_9^{\rm NP} = -C_9'$	$(C_9^{\rm NP}, C_{10}^{\rm NP})$	$(C_9^{\rm NP}, C_9')$	$(C_9^{\rm NP}, C_{10}')$
[0.10, 0.98]	0.114 ± 0.021	0.106 ± 0.019	0.104 ± 0.019	0.102 ± 0.019	0.097 ± 0.018	0.103 ± 0.019	0.099 ± 0.018	0.098 ± 0.018
[1.1, 2.5]	0.105 ± 0.025	0.090 ± 0.020	0.087 ± 0.021	0.084 ± 0.020	0.077 ± 0.016	0.086 ± 0.019	0.080 ± 0.017	0.077 ± 0.016
[2.5, 4.0]	0.110 ± 0.026	0.092 ± 0.021	0.090 ± 0.022	0.086 ± 0.021	0.078 ± 0.017	0.087 ± 0.020	0.081 ± 0.018	0.078 ± 0.017
[4.0, 6.0]	0.153 ± 0.035	0.125 ± 0.028	0.125 ± 0.030	0.119 ± 0.027	0.108 ± 0.023	0.119 ± 0.027	0.111 ± 0.024	0.107 ± 0.023
[1.1, 6.0]	0.368 ± 0.085	0.307 ± 0.068	0.302 ± 0.071	0.290 ± 0.067	0.264 ± 0.055	0.292 ± 0.065	0.271 ± 0.057	0.262 ± 0.056
[0.045, 6.0]	0.512 ± 0.103	0.440 ± 0.083	0.434 ± 0.086	0.420 ± 0.081	0.388 ± 0.068	0.423 ± 0.080	0.398 ± 0.071	0.387 ± 0.069

TABLE X. The binned average central values and the corresponding 1σ uncertainties for the normalized longitudinal polarization fraction $\langle F_L \rangle$ of $B_s \to f_2'(1525)(\to K^+K^-)\mu^+\mu^-$ decays in the SM and in several NP cases.

q^2 bins (GeV^2)	$\langle F_L \rangle$							
	SM	$C_9^{\rm NP}$	$C_{10}^{\rm NP}$	$C_9^{\rm NP} = -C_{10}^{\rm NP}$	$C_9^{\rm NP} = -C_9'$	$(C_9^{\rm NP}, C_{10}^{\rm NP})$	$(C_9^{\rm NP}, C_9')$	$(C_9^{\rm NP}, C_{10}')$
[0.10, 0.98]	0.503 ± 0.108	0.436 ± 0.105	0.462 ± 0.110	0.439 ± 0.107	0.386 ± 0.100	0.429 ± 0.105	0.394 ± 0.101	0.385 ± 0.101
[1.1, 2.5]	0.855 ± 0.047	0.799 ± 0.061	0.856 ± 0.051	0.827 ± 0.058	0.758 ± 0.069	0.804 ± 0.062	0.764 ± 0.068	0.757 ± 0.071
[2.5, 4.0]	0.843 ± 0.045	0.811 ± 0.049	0.861 ± 0.041	0.840 ± 0.044	0.769 ± 0.058	0.819 ± 0.048	0.780 ± 0.055	0.777 ± 0.057
[4.0, 6.0]	0.762 ± 0.062	0.745 ± 0.062	0.780 ± 0.061	0.767 ± 0.061	0.698 ± 0.070	0.752 ± 0.062	0.714 ± 0.067	0.713 ± 0.068
[1.1, 6.0]	0.812 ± 0.050	0.779 ± 0.054	0.825 ± 0.047	0.805 ± 0.050	0.735 ± 0.062	0.786 ± 0.053	0.747 ± 0.060	0.744 ± 0.061
[0.045, 6.0]	0.712 ± 0.069	0.662 ± 0.077	0.700 ± 0.074	0.677 ± 0.077	0.611 ± 0.081	0.662 ± 0.078	0.622 ± 0.080	0.615 ± 0.083

TABLE XI. The binned average central values and the corresponding 1σ uncertainties for the normalized forward-backward asymmetry $\langle A_{FB} \rangle$ of $B_s \to f_2'(1525)(\to K^+K^-)\mu^+\mu^-$ decays in the SM and in several NP cases.

q^2 bins (GeV^2)	$\langle A_{FB} \rangle$							
	SM	$C_9^{\rm NP}$	$C_{10}^{\rm NP}$	$C_9^{\rm NP} = -C_{10}^{\rm NP}$	$C_9^{\rm NP} = -C_9'$	$(C_9^{\rm NP}, C_{10}^{\rm NP})$	$(C_9^{\rm NP}, C_9')$	$(C_9^{\rm NP}, C_{10}')$
[0.10, 0.98]	0.086 ± 0.016	0.098 ± 0.016	0.079 ± 0.013	0.087 ± 0.014	0.106 ± 0.016	0.094 ± 0.015	0.105 ± 0.016	0.106 ± 0.017
[1.1, 2.5]	0.082 ± 0.036	0.127 ± 0.042	0.083 ± 0.036	0.105 ± 0.039	0.148 ± 0.045	0.123 ± 0.041	0.149 ± 0.045	0.156 ± 0.047
[2.5, 4.0]	-0.014 ± 0.039	0.040 ± 0.042	-0.015 ± 0.040	0.010 ± 0.042	0.049 ± 0.048	0.033 ± 0.042	0.057 ± 0.046	0.065 ± 0.048
[4.0, 6.0]	-0.116 ± 0.049	-0.063 ± 0.047	-0.119 ± 0.051	-0.097 ± 0.050	-0.068 ± 0.053	-0.072 ± 0.049	-0.054 ± 0.051	-0.049 ± 0.051
[1.1, 6.0]	-0.030 ± 0.040	0.023 ± 0.041	-0.030 ± 0.040	-0.007 ± 0.041	0.029 ± 0.046	0.016 ± 0.041	0.038 ± 0.044	0.045 ± 0.046
[0.045, 6.0]	-0.000 ± 0.030	0.042 ± 0.030	-0.000 ± 0.030	0.019 ± 0.030	0.048 ± 0.032	0.036 ± 0.030	0.054 ± 0.031	0.059 ± 0.032

TABLE XII. The binned average central values and the corresponding 1σ uncertainties for $\langle P_1 \rangle$ of $B_s \to f_2'(1525)(\to K^+K^-)\mu^+\mu^-$ decays in the SM and in several NP cases.

	$\langle P_1 \rangle$							
q^2 bins (GeV^2)	SM	$C_9^{\rm NP}$	$C_{10}^{\rm NP}$	$C_9^{\rm NP} = -C_{10}^{\rm NP}$	$C_9^{\rm NP} = -C_9'$	$(C_9^{\rm NP}, C_{10}^{\rm NP})$	$(C_9^{\rm NP}, C_9')$	$(C_9^{\rm NP}, C_{10}')$
[0.10, 0.98]	-0.008 ± 0.267	-0.010 ± 0.259	-0.007 ± 0.270	-0.009 ± 0.265	-0.077 ± 0.258	-0.010 ± 0.261	-0.051 ± 0.257	-0.004 ± 0.257
[1.1, 2.5]	-0.043 ± 0.197	-0.041 ± 0.203	-0.034 ± 0.224	-0.036 ± 0.217	-0.224 ± 0.192	-0.039 ± 0.209	-0.156 ± 0.198	0.052 ± 0.204
[2.5, 4.0]	-0.112 ± 0.240	-0.102 ± 0.204	-0.109 ± 0.241	-0.104 ± 0.218	-0.166 ± 0.212	-0.102 ± 0.206	-0.148 ± 0.201	0.069 ± 0.198
[4.0, 6.0]	-0.159 ± 0.282	-0.154 ± 0.256	-0.161 ± 0.297	-0.158 ± 0.277	-0.090 ± 0.264	-0.155 ± 0.261	-0.120 ± 0.256	0.024 ± 0.254
[1.1, 6.0]	-0.121 ± 0.222	-0.110 ± 0.196	-0.117 ± 0.219	-0.112 ± 0.204	-0.141 ± 0.201	-0.110 ± 0.196	-0.135 ± 0.193	0.043 ± 0.193
[0.045, 6.0]	-0.074 ± 0.175	-0.067 ± 0.177	-0.066 ± 0.178	-0.064 ± 0.179	-0.106 ± 0.176	-0.065 ± 0.178	-0.094 ± 0.176	0.024 ± 0.178

TABLE XIII. The binned average central values and the corresponding 1σ uncertainties for $\langle P_2 \rangle$ of $B_s \to f_2'(1525)(\to K^+K^-)\mu^+\mu^-$ decays in the SM and in several NP cases.

	$\langle P_2 \rangle$							
q^2 bins (GeV^2)	SM	$C_9^{\rm NP}$	$C_{10}^{\rm NP}$	$C_9^{\rm NP} = -C_{10}^{\rm NP}$	$C_9^{\rm NP} = -C_9'$	$(C_9^{\rm NP}, C_{10}^{\rm NP})$	$(C_9^{\rm NP}, C_9')$	$(C_9^{\rm NP}, C_{10}')$
[0.10, 0.98]	0.158 ± 0.029	0.156 ± 0.029	0.133 ± 0.025	0.141 ± 0.026	0.155 ± 0.028	0.149 ± 0.028	0.155 ± 0.028	0.154 ± 0.029
[1.1, 2.5]	0.378 ± 0.081	0.429 ± 0.038	0.383 ± 0.070	0.409 ± 0.050	0.416 ± 0.042	0.425 ± 0.039	0.428 ± 0.035	0.436 ± 0.031
[2.5, 4.0]	-0.046 ± 0.158	0.148 ± 0.143	-0.054 ± 0.181	0.053 ± 0.169	0.148 ± 0.136	0.129 ± 0.151	0.179 ± 0.135	0.197 ± 0.134
[4.0, 6.0]	-0.315 ± 0.082	-0.154 ± 0.104	-0.351 ± 0.086	-0.266 ± 0.101	-0.142 ± 0.102	-0.184 ± 0.106	-0.116 ± 0.106	-0.104 ± 0.108
[1.1, 6.0]	-0.098 ± 0.128	0.072 ± 0.119	-0.109 ± 0.141	-0.019 ± 0.135	0.076 ± 0.115	0.052 ± 0.125	0.103 ± 0.114	0.118 ± 0.113
[0.045, 6.0]	-0.003 ± 0.085	0.098 ± 0.063	-0.006 ± 0.084	0.044 ± 0.074	0.100 ± 0.062	0.085 ± 0.066	0.116 ± 0.058	0.124 ± 0.056

TABLE XIV. The binned average central values and the corresponding 1σ uncertainties for $\langle P_4' \rangle$ of $B_s \to f_2'(1525)(\to K^+K^-)\mu^+\mu^-$ decays in the SM and in several NP cases.

	$\langle P_4' \rangle$							
q^2 bins (GeV^2)	SM	$C_9^{\rm NP}$	$C_{10}^{\rm NP}$	$C_9^{\rm NP} = -C_{10}^{\rm NP}$	$C_9^{\rm NP} = -C_9'$	$(C_9^{\rm NP}, C_{10}^{\rm NP})$	$(C_9^{\rm NP}, C_9')$	$(C_9^{\rm NP}, C_{10}')$
[0.10, 0.98]	-0.457 ± 0.089	-0.351 ± 0.069	-0.552 ± 0.095	-0.475 ± 0.083	-0.199 ± 0.050	-0.394 ± 0.073	-0.239 ± 0.054	-0.372 ± 0.065
[1.1, 2.5]	0.251 ± 0.234	0.256 ± 0.186	0.090 ± 0.256	0.140 ± 0.221	0.351 ± 0.152	0.207 ± 0.195	0.318 ± 0.158	0.166 ± 0.169
[2.5, 4.0]	0.811 ± 0.197	0.760 ± 0.181	0.753 ± 0.230	0.737 ± 0.211	0.761 ± 0.159	0.743 ± 0.191	0.756 ± 0.164	0.643 ± 0.182
[4.0, 6.0]	0.995 ± 0.156	0.968 ± 0.150	0.983 ± 0.170	0.970 ± 0.163	0.918 ± 0.150	0.964 ± 0.155	0.935 ± 0.149	0.867 ± 0.161
[1.1, 6.0]	0.739 ± 0.188	0.702 ± 0.173	0.668 ± 0.215	0.666 ± 0.199	0.707 ± 0.152	0.681 ± 0.182	0.703 ± 0.157	0.597 ± 0.173
[0.045, 6.0]	0.405 ± 0.183	0.395 ± 0.161	0.297 ± 0.198	0.320 ± 0.181	0.439 ± 0.135	0.361 ± 0.167	0.423 ± 0.141	0.315 ± 0.152

TABLE XV. The binned average central values and the corresponding 1σ uncertainties for $\langle P_5' \rangle$ of $B_s \to f_2'(1525)(\to K^+K^-)\mu^+\mu^-$ decays in the SM and in several NP cases.

	$\langle P_5' \rangle$							
q^2 bins (GeV^2)	SM	$C_9^{\rm NP}$	$C_{10}^{\rm NP}$	$C_9^{\rm NP} = -C_{10}^{\rm NP}$	$C_9^{\rm NP} = -C_9'$	$(C_9^{\rm NP}, C_{10}^{\rm NP})$	$(C_9^{\rm NP}, C_9')$	$(C_9^{\rm NP}, C_{10}')$
[0.10, 0.98]	0.593 ± 0.114	0.709 ± 0.116	0.545 ± 0.104	0.620 ± 0.109	0.786 ± 0.132	0.684 ± 0.114	0.777 ± 0.126	0.700 ± 0.115
[1.1, 2.5]	-0.079 ± 0.267	0.172 ± 0.230	-0.086 ± 0.272	0.038 ± 0.253	0.199 ± 0.249	0.141 ± 0.236	0.233 ± 0.235	0.163 ± 0.226
[2.5, 4.0]	-0.620 ± 0.236	-0.354 ± 0.23	-0.670 ± 0.255	-0.534 ± 0.253	-0.366 ± 0.247	-0.403 ± 0.243	-0.310 ± 0.242	-0.358 ± 0.233
[4.0, 6.0]	-0.797 ± 0.187	-0.615 ± 0.187	-0.842 ± 0.196	-0.763 ± 0.197	-0.655 ± 0.189	-0.662 ± 0.193	-0.599 ± 0.190	-0.631 ± 0.183
[1.1, 6.0]	-0.552 ± 0.220	-0.316 ± 0.219	-0.580 ± 0.232	-0.469 ± 0.233	-0.329 ± 0.233	-0.358 ± 0.226	-0.277 ± 0.227	-0.322 ± 0.219
[0.045, 6.0]	-0.238 ± 0.204	-0.036 ± 0.194	-0.237 ± 0.204	-0.148 ± 0.203	-0.029 ± 0.211	-0.064 ± 0.198	0.008 ± 0.202	-0.041 ± 0.195

TABLE XVI. The binned average central values and the corresponding 1σ uncertainties for the ratio of branching ratio $\langle R_{f_2'} \rangle$ of $B_s \to f_2'(1525)(\to K^+K^-)\mu^+\mu^-$ decays in the SM and in several NP cases.

	$\langle R_{f_2'} \rangle$							
q^2 bins (GeV^2)	SM	$C_9^{\rm NP}$	$C_{10}^{\rm NP}$	$C_9^{\rm NP} = -C_{10}^{\rm NP}$	$C_9^{\rm NP} = -C_9'$	$(C_9^{\rm NP}, C_{10}^{\rm NP})$	$(C_9^{\rm NP}, C_9')$	$(C_9^{\rm NP}, C_{10}')$
[0.10, 0.98]	0.979 ± 0.005	0.910 ± 0.025	0.893 ± 0.015	0.882 ± 0.022	0.839 ± 0.044	0.890 ± 0.027	0.857 ± 0.040	0.846 ± 0.040
[1.1, 2.5]	0.994 ± 0.005	0.854 ± 0.022	0.826 ± 0.010	0.803 ± 0.012	0.735 ± 0.037	0.815 ± 0.019	0.761 ± 0.035	0.737 ± 0.030
[2.5, 4.0]	0.995 ± 0.005	0.829 ± 0.014	0.810 ± 0.012	0.779 ± 0.006	0.713 ± 0.028	0.788 ± 0.010	0.734 ± 0.024	0.707 ± 0.019
[4.0, 6.0]	0.996 ± 0.003	0.816 ± 0.009	0.810 ± 0.011	0.773 ± 0.005	0.708 ± 0.025	0.776 ± 0.005	0.723 ± 0.019	0.697 ± 0.015
[1.1, 6.0]	0.995 ± 0.002	0.831 ± 0.014	0.814 ± 0.010	0.783 ± 0.005	0.717 ± 0.028	0.790 ± 0.010	0.737 ± 0.024	0.711 ± 0.020
[0.045, 6.0]	0.976 ± 0.005	0.842 ± 0.016	0.827 ± 0.007	0.802 ± 0.010	0.744 ± 0.033	0.809 ± 0.015	0.762 ± 0.029	0.742 ± 0.026

TABLE XVII. The binned average central values and the corresponding 1σ uncertainties for $\langle Q_1 \rangle$ of $B_s \to f_2'(1525)(\to K^+K^-)\mu^+\mu^-$ decays in the SM and in several NP cases.

	$\langle Q_1 \rangle$							
q^2 bins (GeV^2)	SM	$C_9^{\rm NP}$	$C_{10}^{\rm NP}$	$C_9^{\rm NP} = -C_{10}^{\rm NP}$	$C_9^{\rm NP} = -C_9'$	$(C_9^{\rm NP}, C_{10}^{\rm NP})$	$(C_9^{\rm NP}, C_9')$	$(C_9^{\rm NP}, C_{10}')$
[0.10, 0.98]	0.000 ± 0.003	-0.002 ± 0.008	0.001 ± 0.008	-0.000 ± 0.001	-0.069 ± 0.016	-0.002 ± 0.005	-0.043 ± 0.013	0.004 ± 0.011
[1.1, 2.5]	-0.000 ± 0.001	0.002 ± 0.028	0.010 ± 0.051	0.007 ± 0.045	-0.181 ± 0.032	0.004 ± 0.036	-0.113 ± 0.032	0.095 ± 0.046
[2.5, 4.0]	-0.000 ± 0.000	0.009 ± 0.060	0.003 ± 0.017	0.007 ± 0.039	-0.055 ± 0.079	0.010 ± 0.059	-0.037 ± 0.075	0.181 ± 0.076
[4.0, 6.0]	-0.000 ± 0.000	0.006 ± 0.035	-0.002 ± 0.019	0.002 ± 0.009	0.069 ± 0.054	0.005 ± 0.028	0.039 ± 0.047	0.183 ± 0.046
[1.1, 6.0]	-0.001 ± 0.002	0.010 ± 0.048	0.003 ± 0.014	0.008 ± 0.035	-0.021 ± 0.066	0.011 ± 0.049	-0.014 ± 0.062	0.163 ± 0.062
[0.045, 6.0]	-0.014 ± 0.040	-0.007 ± 0.009	-0.005 ± 0.016	-0.004 ± 0.006	-0.046 ± 0.032	-0.005 ± 0.003	-0.034 ± 0.019	0.084 ± 0.021

TABLE XVIII. The binned average central values and the corresponding 1σ uncertainties for $\langle Q_2 \rangle$ of $B_s \to f_2'(1525)(\to K^+K^-)\mu^+\mu^-$ decays in the SM and in several NP cases.

	$\langle Q_2 \rangle$							
q^2 bins (GeV^2)	SM	$C_9^{\rm NP}$	$C_{10}^{\rm NP}$	$C_9^{\rm NP} = -C_{10}^{\rm NP}$	$C_9^{\rm NP} = -C_9'$	$(C_9^{\rm NP}, C_{10}^{\rm NP})$	$(C_9^{\rm NP}, C_9')$	$(C_9^{\rm NP}, C_{10}')$
[0.10, 0.98]	0.026 ± 0.005	0.023 ± 0.004	0.001 ± 0.001	0.008 ± 0.002	0.022 ± 0.005	0.016 ± 0.003	0.022 ± 0.004	0.022 ± 0.005
[1.1, 2.5]	0.005 ± 0.002	0.056 ± 0.049	0.010 ± 0.019	0.036 ± 0.038	0.043 ± 0.052	0.051 ± 0.049	0.055 ± 0.057	0.063 ± 0.060
[2.5, 4.0]	-0.001 ± 0.001	0.193 ± 0.025	-0.008 ± 0.025	0.098 ± 0.018	0.194 ± 0.030	0.175 ± 0.021	0.225 ± 0.033	0.243 ± 0.036
[4.0, 6.0]	-0.001 ± 0.001	0.160 ± 0.030	-0.037 ± 0.007	0.048 ± 0.021	0.172 ± 0.031	0.130 ± 0.030	0.198 ± 0.034	0.210 ± 0.040
[1.1, 6.0]	-0.003 ± 0.001	0.167 ± 0.017	-0.014 ± 0.013	0.076 ± 0.012	0.171 ± 0.020	0.147 ± 0.015	0.198 ± 0.022	0.213 ± 0.027
[0.045, 6.0]	-0.007 ± 0.019	0.095 ± 0.005	-0.009 ± 0.017	0.041 ± 0.008	0.096 ± 0.007	0.082 ± 0.004	0.112 ± 0.010	0.121 ± 0.014

TABLE XIX. The binned average central values and the corresponding 1σ uncertainties for $\langle Q_4' \rangle$ of $B_s \to f_2'(1525)(\to K^+K^-)\mu^+\mu^-$ decays in the SM and in several NP cases.

	$\langle Q_4' \rangle$							
q^2 bins (GeV^2)	SM	$C_9^{\rm NP}$	$C_{10}^{\rm NP}$	$C_9^{\rm NP} = -C_{10}^{\rm NP}$	$C_9^{\rm NP} = -C_9'$	$(C_9^{\rm NP}, C_{10}^{\rm NP})$	$(C_9^{\rm NP}, C_9')$	$(C_9^{\rm NP}, C_{10}')$
[0.10, 0.98]	0.011 ± 0.005	0.116 ± 0.022	-0.084 ± 0.012	-0.007 ± 0.005	0.268 ± 0.052	0.073 ± 0.016	0.228 ± 0.045	0.096 ± 0.026
[1.1, 2.5]	0.002 ± 0.001	0.007 ± 0.050	-0.159 ± 0.029	-0.109 ± 0.017	0.102 ± 0.090	-0.042 ± 0.041	0.070 ± 0.082	-0.082 ± 0.068
[2.5, 4.0]	0.000 ± 0.000	-0.050 ± 0.024	-0.058 ± 0.039	-0.073 ± 0.025	-0.049 ± 0.045	-0.068 ± 0.021	-0.054 ± 0.039	-0.167 ± 0.028
[4.0, 6.0]	0.000 ± 0.000	-0.027 ± 0.014	-0.012 ± 0.017	-0.025 ± 0.014	-0.077 ± 0.016	-0.031 ± 0.014	-0.060 ± 0.014	-0.128 ± 0.021
[1.1, 6.0]	0.004 ± 0.001	-0.033 ± 0.020	-0.067 ± 0.032	-0.069 ± 0.019	-0.028 ± 0.044	-0.054 ± 0.016	-0.032 ± 0.037	-0.138 ± 0.023
[0.045, 6.0]	0.098 ± 0.015	0.088 ± 0.016	-0.010 ± 0.027	0.013 ± 0.010	0.132 ± 0.047	0.054 ± 0.010	0.117 ± 0.039	0.008 ± 0.023

TABLE XX. The binned average central values and the corresponding 1σ uncertainties for $\langle Q_5' \rangle$ of $B_s \to f_2'(1525)(\to K^+K^-)\mu^+\mu^-$ decays in the SM and in several NP cases.

	$\langle Q_5' \rangle$							
q^2 bins (GeV^2)	SM	$C_9^{\rm NP}$	$C_{10}^{\rm NP}$	$C_9^{\rm NP} = -C_{10}^{\rm NP}$	$C_9^{\rm NP} = -C_9'$	$(C_9^{\rm NP}, C_{10}^{\rm NP})$	$(C_9^{\rm NP}, C_9')$	$(C_9^{\rm NP}, C_{10}')$
[0.10, 0.98]	0.039 ± 0.011	0.155 ± 0.016	-0.009 ± 0.004	0.066 ± 0.007	0.232 ± 0.033	0.129 ± 0.013	0.223 ± 0.027	0.145 ± 0.014
[1.1, 2.5]	-0.002 ± 0.004	0.248 ± 0.040	-0.009 ± 0.012	0.115 ± 0.016	0.276 ± 0.031	0.217 ± 0.033	0.309 ± 0.041	0.240 ± 0.042
[2.5, 4.0]	-0.004 ± 0.002	0.261 ± 0.043	-0.054 ± 0.021	0.082 ± 0.029	0.249 ± 0.052	0.212 ± 0.040	0.306 ± 0.054	0.258 ± 0.052
[4.0, 6.0]	-0.004 ± 0.001	0.179 ± 0.041	-0.049 ± 0.016	0.031 ± 0.018	0.139 ± 0.055	0.132 ± 0.036	0.195 ± 0.056	0.163 ± 0.054
[1.1, 6.0]	-0.007 ± 0.002	0.229 ± 0.035	-0.035 ± 0.014	0.076 ± 0.023	0.217 ± 0.044	0.187 ± 0.032	0.269 ± 0.045	0.224 ± 0.043
[0.045, 6.0]	-0.071 ± 0.021	0.131 ± 0.015	-0.070 ± 0.020	0.019 ± 0.018	0.139 ± 0.029	0.103 ± 0.016	0.175 ± 0.023	0.126 ± 0.017

TABLE XXI. The binned average central values and the corresponding 1σ uncertainties for $\langle Q_{A_{FB}} \rangle$ of $B_s \to f_2'(1525)(\to K^+K^-)\mu^+\mu^-$ decays in the SM and in several NP cases.

	$\langle Q_{A_{FB}} \rangle$							
q^2 bins (GeV^2)	SM	$C_9^{\rm NP}$	$C_{10}^{\rm NP}$	$C_9^{\rm NP} = -C_{10}^{\rm NP}$	$C_9^{\rm NP} = -C_9'$	$(C_9^{\rm NP}, C_{10}^{\rm NP})$	$(C_9^{\rm NP}, C_9')$	$(C_9^{\rm NP}, C_{10}')$
[0.10, 0.98]	-0.010 ± 0.002	0.001 ± 0.003	-0.018 ± 0.004	-0.009 ± 0.004	0.010 ± 0.005	-0.002 ± 0.004	0.008 ± 0.005	0.010 ± 0.005
[1.1, 2.5]	-0.002 ± 0.001	0.043 ± 0.010	-0.002 ± 0.001	0.021 ± 0.006	0.064 ± 0.013	0.039 ± 0.010	0.064 ± 0.014	0.072 ± 0.017
[2.5, 4.0]	0.000 ± 0.001	0.055 ± 0.015	-0.000 ± 0.001	0.025 ± 0.007	0.063 ± 0.017	0.048 ± 0.013	0.072 ± 0.019	0.079 ± 0.022
[4.0, 6.0]	0.001 ± 0.000	0.054 ± 0.014	-0.002 ± 0.002	0.020 ± 0.005	0.048 ± 0.017	0.044 ± 0.012	0.062 ± 0.018	0.068 ± 0.021
[1.1, 6.0]	-0.000 ± 0.001	0.052 ± 0.013	-0.001 ± 0.001	0.023 ± 0.006	0.058 ± 0.016	0.045 ± 0.012	0.067 ± 0.017	0.074 ± 0.020
[0.045, 6.0]	-0.004 ± 0.001	0.038 ± 0.008	-0.004 ± 0.001	0.015 ± 0.003	0.045 ± 0.009	0.032 ± 0.007	0.050 ± 0.010	0.056 ± 0.012

TABLE XXII. The binned average central values and the corresponding 1σ uncertainties for $\langle Q_{F_L} \rangle$ of $B_s \to f_2'(1525)(\to K^+K^-)\mu^+\mu^-$ decays in the SM and in several NP cases.

	$\langle Q_{F_L} \rangle$						
q^2 bins (GeV^2)	SM	C_9^{NP}	C_{10}^{NP}	$C_9^{\mathrm{NP}} = -C_{10}^{\mathrm{NP}}$	$C_9^{\mathrm{NP}} = -C_9'$	$(C_9^{\mathrm{NP}}, C_{10}^{\mathrm{NP}})$	$(C_9^{\mathrm{NP}}, C_9')$	$(C_9^{\mathrm{NP}}, C_{10}')$
[0.10, 0.98]	0.001 ± 0.001	-0.066 ± 0.005	-0.040 ± 0.004	-0.063 ± 0.004	-0.116 ± 0.011	-0.073 ± 0.005	-0.107 ± 0.010	-0.117 ± 0.009
[1.1, 2.5]	0.002 ± 0.001	-0.054 ± 0.015	0.003 ± 0.009	-0.026 ± 0.013	-0.095 ± 0.023	-0.049 ± 0.015	-0.089 ± 0.022	-0.096 ± 0.025
[2.5, 4.0]	0.002 ± 0.001	-0.030 ± 0.010	0.020 ± 0.005	-0.001 ± 0.006	-0.072 ± 0.018	-0.021 ± 0.010	-0.061 ± 0.016	-0.064 ± 0.019
[4.0, 6.0]	0.002 ± 0.000	-0.016 ± 0.006	0.020 ± 0.003	0.007 ± 0.002	-0.062 ± 0.016	-0.008 ± 0.005	-0.046 ± 0.011	-0.047 ± 0.014
[1.1, 6.0]	0.002 ± 0.001	-0.030 ± 0.010	0.015 ± 0.004	-0.005 ± 0.007	-0.075 ± 0.017	-0.023 ± 0.010	-0.063 ± 0.015	-0.066 ± 0.018
[0.045, 6.0]	0.012 ± 0.002	-0.038 ± 0.007	-0.001 ± 0.006	-0.023 ± 0.008	-0.089 ± 0.012	-0.038 ± 0.009	-0.078 ± 0.011	-0.085 ± 0.014

APPENDIX B: HELICITY AMPLITUDES

In the process of $B_s \to f_2'(1525)(\to K^+K^-)l^+l^-$ decays, initially the B_s meson decays into an on-shell strange meson along with a pair of leptons. Further, the $f_2'(1525)$ decays strongly into K^+K^-. This multibody decay evaluated in the helicity framework which uses the metric tensor

$$g_{\mu\nu} = -\sum_{\lambda} \epsilon_\mu(\lambda)\epsilon_\nu^*(\lambda) + \frac{q_\mu q_\nu}{q^2}, \tag{B1}$$

where ϵ is the polarization vector with the momentum q and where λ is the three kinds of polarizations. Here, the metric tensor $g_{\mu\nu}$ is expressed as a summation of four polarizations where the last term is identified to be the timelike polarization $\epsilon_\mu(t) = q^\mu/q^2$. In the SM, the production of lepton pairs in the final state is due to a Z boson, an off-shell photon, or any hadronic meson. Although, the coupling strengths of these states may be different, they processe the similar Lorentz structure of type V-A, V + A, or a combination of both. Hence, the decay amplitude for $B_s \to f_2' l^+ l^-$ is written as

$$\mathcal{A}(B_s \to f_2' l^+ l^-) = \mathcal{L}^\mu(L)\mathcal{H}_\mu(L) + \mathcal{L}^\mu(R)\mathcal{H}_\mu(R), \tag{B2}$$

where $\mathcal{L}^\mu(L) = \bar{l}\gamma_\mu(1-\gamma_5)l$ and $\mathcal{L}^\mu(R) = \bar{l}\gamma_\mu(1+\gamma_5)l$ are the lepton pair spinor products and, similarly, $\mathcal{H}$ includes $B_s \to f_2'$. Further, the factorization of the decay amplitude is obtained as

$$\begin{aligned}\mathcal{A}(B_s \to f_2' l^+ l^-) &= \mathcal{L}^\mu(L)\mathcal{H}_\mu(L)g_{\mu\nu} + \mathcal{L}^\mu(R)\mathcal{H}_\mu(R)g_{\mu\nu} \\ &= -\sum_{\lambda} \mathcal{L}_{L\lambda}\mathcal{H}_{L\lambda} - \sum_{\lambda} \mathcal{L}_{R\lambda}\mathcal{H}_{R\lambda}.\end{aligned} \tag{B3}$$

The Lorentz invariant amplitude for the lepton part $\mathcal{L}_{L\lambda} = \mathcal{L}^\mu(L)\epsilon_\mu(\lambda)$ and $\mathcal{L}_{R\lambda} = \mathcal{L}^\mu(R)\epsilon_\mu(\lambda)$ and similarly for the hadronic part. The timelike polarization vanishes at $m_l = 0$ for $l = e,\ \mu$. Using the equation of motion, this term is proportional to the lepton mass. Since the hadronic and leptonic amplitudes are Lorentz invariant, it allows us to evaluate in the different frames. Due to many similarities between K^*, K_2^*, and f_2', the differential decay width for $B_s \to f_2' l^+ l^-$ are simply obtained in a comparative manner by multiplying the factors $\frac{\sqrt{\lambda}}{\sqrt{8}m_B m_{f_2'}}$ and $\frac{\sqrt{\lambda}}{\sqrt{6}m_B m_{f_2'}}$ respectively with the longitudinal and transverse amplitudes. This modification is because since we replace the polarization vector ϵ by ϵ_T in the definition of $B \to T$ form factors. Explicitly, the expressions for the hadronic amplitudes are written as [19]

$$
\begin{aligned}
H_{L0} &= N_{f_2'}\frac{\sqrt{\lambda}}{\sqrt{8}m_{B_s}m_{f_2'}}\frac{1}{2m_{f_2'}\sqrt{q^2}}\left\{(C_9^{\rm eff}-C_{10})\left[(m_{B_s}^2-m_{f_2'}^2-q^2)(m_{B_s}+m_{f_2'})A_1-\frac{\lambda}{m_{B_s}+m_{f_2'}}A_2\right]\right.\\
&\left.+2m_bC_7^{\rm eff}\left[(m_{B_s}^2+3m_{f_2'}^2-q^2)T_2-\frac{\lambda}{m_{B_s}^2-m_{f_2'}^2}T_3\right]\right\},\\
H_{L\perp} &= -N_{f_2'}\sqrt{2}\frac{\sqrt{\lambda}}{\sqrt{6}m_{B_s}m_{f_2'}}\left[(C_9^{\rm eff}-C_{10})\frac{\sqrt{\lambda}}{m_{B_s}+m_{f_2'}}V+\frac{\sqrt{\lambda}2m_bC_7^{\rm eff}}{q^2}T_1\right],\\
H_{L\parallel} &= N_{f_2'}\sqrt{2}\frac{\sqrt{\lambda}}{\sqrt{6}m_{B_s}m_{f_2'}}\left[(C_9^{\rm eff}-C_{10})(m_{B_s}+m_{f_2'})A_1+\frac{2m_bC_7^{\rm eff}(m_{B_s}^2-m_{f_2'}^2)}{q^2}T_2\right],\\
H_{Lt} &= N_{f_2'}\frac{\sqrt{\lambda}}{\sqrt{8}m_{B_s}m_{f_2'}}(C_9^{\rm eff}-C_{10})\frac{\sqrt{\lambda}}{\sqrt{q^2}}A_0.
\end{aligned}
\tag{B4}
$$

The spherical harmonic functions for K^* and f_2' are related as

$$
\begin{aligned}
\sqrt{\frac{3}{4\pi}}\cos(\theta_K) \equiv C(K^*) &\to \sqrt{\frac{5}{16\pi}}(3\cos^2\theta_K-1) \equiv C(f_2'),\\
\sqrt{\frac{3}{8\pi}}\sin(\theta_K) \equiv S(K^*) &\to \sqrt{\frac{15}{32\pi}}\sin(2\theta_K) \equiv S(f_2').
\end{aligned}
\tag{B5}
$$

The amplitude equations and the branching fraction formulas are compatible with Refs. [19,22].

[1] R. Aaij *et al.* (LHCb Collaboration), Search for Lepton-Universality Violation in $B^+ \to K^+\ell^+\ell^-$ decays, Phys. Rev. Lett. **122**, 191801 (2019).

[2] G. Hiller and F. Kruger, More model-independent analysis of $b \to s$ processes, Phys. Rev. D **69**, 074020 (2004).

[3] M. Bordone, G. Isidori, and A. Pattori, On the Standard Model predictions for R_K and R_{K^*}, Eur. Phys. J. C **76**, 440 (2016).

[4] R. Aaij *et al.* (LHCb Collaboration), Test of lepton universality with $B^0 \to K^{*0}\ell^+\ell^-$ decays, J. High Energy Phys. 08 (2017) 055.

[5] R. Aaij *et al.* (LHCb Collaboration), Measurement of *CP*-Averaged Observables in the $B^0 \to K^{*0}\mu^+\mu^-$ Decay, Phys. Rev. Lett. **125**, 011802 (2020).

[6] A. Abdesselam *et al.* (Belle Collaboration), Test of lepton flavor universality in $B \to K^*\ell^+\ell^-$ decays at Belle, arXiv:1904.02440.

[7] S. Descotes-Genon, J. Matias, M. Ramon, and J. Virto, Implications from clean observables for the binned analysis of $B \to K*\mu^+\mu^-$ at large recoil, J. High Energy Phys. 01 (2013) 048.

[8] S. Descotes-Genon, T. Hurth, J. Matias, and J. Virto, Optimizing the basis of $B \to K^*ll$ observables in the full kinematic range, J. High Energy Phys. 05 (2013) 137.

[9] M. Aaboud *et al.* (ATLAS Collaboration), Angular analysis of $B_d^0 \to K^*\mu^+\mu^-$ decays in pp collisions at $\sqrt{s} = 8$ TeV with the ATLAS detector, J. High Energy Phys. 10 (2018) 047.

[10] R. Aaij *et al.* (LHCb Collaboration), Measurement of Form-Factor-Independent Observables in the Decay $B^0 \to K^{*0}\mu^+\mu^-$, Phys. Rev. Lett. **111**, 191801 (2013).

[11] R. Aaij *et al.* (LHCb Collaboration), Angular analysis of the $B^0 \to K^{*0}\mu^+\mu^-$ decay using 3 fb^{-1} of integrated luminosity, J. High Energy Phys. 02 (2016) 104.

[12] J. Aebischer, J. Kumar, P. Stangl, and D. M. Straub, A Global Likelihood for Precision Constraints and Flavour Anomalies, Eur. Phys. J. C **79**, 509 (2019).

[13] CMS Collaboration, Measurement of the P_1 and P_5' angular parameters of the decay $B^0 \to K^{*0}\mu^+\mu^-$ in proton-proton collisions at $\sqrt{s} = 8$ TeV, Report No. CMS-PAS-BPH-15-008.

[14] A. Abdesselam *et al.* (Belle Collaboration), Angular analysis of $B^0 \to K^*(892)^0\ell^+\ell^-$, arXiv:1604.04042.

[15] S. Descotes-Genon, L. Hofer, J. Matias, and J. Virto, On the impact of power corrections in the prediction of $B \to K^*\mu^+\mu^-$ observables, J. High Energy Phys. 12 (2014) 125.

[16] R. Aaij *et al.* (LHCb Collaboration), Differential branching fraction and angular analysis of the decay $B_s^0 \to \phi\mu^+\mu^-$, J. High Energy Phys. 07 (2013) 084.

[17] R. Aaij *et al.* (LHCb Collaboration), Angular analysis and differential branching fraction of the decay $B_s^0 \to \phi\mu^+\mu^-$, J. High Energy Phys. 09 (2015) 179.

[18] A. Bharucha, D. M. Straub, and R. Zwicky, $B \to V\ell^+\ell^-$ in the Standard Model from light-cone sum rules, J. High Energy Phys. 08 (2016) 098.

[19] R. H. Li, C. D. Lu, and W. Wang, Branching ratios, forward-backward asymmetries and angular distributions of $B \to K_2^* l^+ l^-$ in the standard model and new physics scenarios, Phys. Rev. D **83**, 034034 (2011).

[20] I. Ahmed, M. J. Aslam, M. Junaid, and S. Shafaq, Model independent analysis of $B \to K_2^*(1430)\mu^+\mu^-$ decay, J. High Energy Phys. 02 (2012) 045.

[21] S. Rai Choudhury, A. S. Cornell, G. C. Joshi, and B. H. J. McKellar, Analysis of the $B \to K*(2)(\to K\,\mathrm{pi})l + l-$ decay, Phys. Rev. D **74**, 054031 (2006).

[22] H. Hatanaka and K. C. Yang, Radiative and semileptonic B decays involving the tensor meson K(2)*(1430) in the Standard model and beyond, Phys. Rev. D **79**, 114008 (2009).

[23] H. Hatanaka and K. C. Yang, Radiative and semileptonic B decays involving higher K-resonances in the final states, Eur. Phys. J. C **67**, 149 (2010).

[24] M. Junaid, M. J. Aslam, and I. Ahmed, Complementarity of semileptonic B to $K_2^*(1430)$ and $K^*(892)$ decays in the Standard Model with fourth generation, Int. J. Mod. Phys. A **27**, 1250149 (2012).

[25] C. D. Lu and W. Wang, Analysis of $B \to K_J^*(\to K\pi)\mu^+\mu^-$ in the higher kaon resonance region, Phys. Rev. D **85**, 034014 (2012).

[26] T. M. Aliev and M. Savci, $B \to K_2 \ell^+\ell^-$ decay beyond the Standard Model, Phys. Rev. D **85**, 015007 (2012).

[27] D. Das, B. Kindra, G. Kumar, and N. Mahajan, $B \to K_2^*(1430)\ell^+\ell^-$ distributions at large recoil in the Standard Model and beyond, Phys. Rev. D **99**, 093012 (2019).

[28] R. Aaij *et al.* (LHCb Collaboration), Observation of $B_s \to J/\psi f_2'(1525)$ in $J/\psi K^+K^-$ Final States, Phys. Rev. Lett. **108**, 151801 (2012).

[29] A. J. Buras and M. Munz, Effective Hamiltonian for $B \to X(s)\, e + e-$ beyond leading logarithms in the NDR and HV schemes, Phys. Rev. D **52**, 186 (1995).

[30] A. Khodjamirian, T. Mannel, A. A. Pivovarov, and Y. M. Wang, Charm-loop effect in $B \to K^{(*)}\ell^+\ell^-$ and $B \to K^*\gamma$, J. High Energy Phys. 09 (2010) 089.

[31] A. Khodjamirian, T. Mannel, and Y. M. Wang, $B \to K\ell^+\ell^-$ decay at large hadronic recoil, J. High Energy Phys. 02 (2013) 010.

[32] C. Bobeth, M. Chrzaszcz, D. van Dyk, and J. Virto, Long-distance effects in $B \to K^*\ell\ell$ from analyticity, Eur. Phys. J. C **78**, 451 (2018).

[33] N. Gubernari, D. van Dyk, and J. Virto, Non-local matrix elements in $B_{(s)} \to \{K^{(*)}, \phi\}\ell^+\ell^-$, J. High Energy Phys. 02 (2021) 088.

[34] A. K. Alok, A. Datta, A. Dighe, M. Duraisamy, D. Ghosh, and D. London, New Physics in $b- > s\mu^+\mu^-$: *CP*-Conserving Observables, J. High Energy Phys. 11 (2011) 121.

[35] A. K. Alok, A. Datta, A. Dighe, M. Duraisamy, D. Ghosh, and D. London, New Physics in b -> s mu+ mu-: *CP*-Violating Observables, J. High Energy Phys. 11 (2011) 122.

[36] D. Bardhan, P. Byakti, and D. Ghosh, Role of tensor operators in R_K and R_{K^*}, Phys. Lett. B **773**, 505 (2017).

[37] A. K. Alok, A. Dighe, S. Gangal, and D. Kumar, Continuing search for new physics in $b \to s\mu\mu$ decays: Two operators at a time, J. High Energy Phys. 06 (2019) 089.

[38] M. Tanabashi *et al.* (Particle Data Group), Review of particle physics, Phys. Rev. D **98**, 030001 (2018).

[39] A. Ali, P. Ball, L. T. Handoko, and G. Hiller, A comparative study of the decays $B \to (K, K^{*})\ell^+\ell^-$ in standard model and supersymmetric theories, Phys. Rev. D **61**, 074024 (2000).

[40] E. R. Berger, A. Donnachie, H. G. Dosch, and O. Nachtmann, Observing the odderon: Tensor meson photoproduction, Eur. Phys. J. C **14**, 673 (2000).

[41] W. Wang, B to tensor meson form factors in the perturbative QCD approach, Phys. Rev. D **83**, 014008 (2011).

[42] S. Cheng, A. Khodjamirian, and J. Virto, $B \to \pi\pi$ form factors from light-cone sum rules with B-meson distribution amplitudes, J. High Energy Phys. 05 (2017) 157.

[43] S. Descotes-Genon, A. Khodjamirian, and J. Virto, Light-cone sum rules for $B \to K\pi$ form factors and applications to rare decays, J. High Energy Phys. 12 (2019) 083.

[44] J. Virto, Anomalies in $b \to s\ell\ell$ transitions and global fits, arXiv:2103.01106.

[45] K. C. Yang, B to light tensor meson form factors derived from light-cone sum rules, Phys. Lett. B **695**, 444 (2011).

[46] D. Becirevic and A. B. Kaidalov, Comment on the heavy → light form-factors, Phys. Lett. B **478**, 417 (2000).

[47] B. Capdevila, S. Descotes-Genon, J. Matias, and J. Virto, Assessing lepton-flavour non-universality from $B \to K^*\ell\ell$ angular analyses, J. High Energy Phys. 10 (2016) 075.

[48] B. Capdevila, A. Crivellin, S. Descotes-Genon, J. Matias, and J. Virto, Patterns of new physics in $b \to s\ell^+\ell^-$ transitions in the light of recent data, J. High Energy Phys. 01 (2018) 093.

[49] W. Altmannshofer, P. Stangl, and D. M. Straub, Interpreting hints for lepton flavor universality violation, Phys. Rev. D **96**, 055008 (2017).

[50] G. D'Amico, M. Nardecchia, P. Panci, F. Sannino, A. Strumia, R. Torre, and A. Urbano, Flavour anomalies after the R_{K^*} measurement, J. High Energy Phys. 09 (2017) 010.

[51] G. Hiller and I. Nisandzic, R_K and R_{K^*} beyond the standard model, Phys. Rev. D **96**, 035003 (2017).

[52] L. S. Geng, B. Grinstein, S. Jger, J. Martin Camalich, X. L. Ren, and R. X. Shi, Towards the discovery of new physics with lepton-universality ratios of $b \to s\ell\ell$ decays, Phys. Rev. D **96**, 093006 (2017).

[53] M. Ciuchini, A. M. Coutinho, M. Fedele, E. Franco, A. Paul, L. Silvestrini, and M. Valli, On Flavourful Easter eggs for New Physics hunger and Lepton Flavour Universality violation, Eur. Phys. J. C **77**, 688 (2017).

[54] A. Celis, J. Fuentes-Martin, A. Vicente, and J. Virto, Gauge-invariant implications of the LHCb measurements on lepton-flavor nonuniversality, Phys. Rev. D **96**, 035026 (2017).

[55] A. K. Alok, B. Bhattacharya, A. Datta, D. Kumar, J. Kumar, and D. London, New physics in $b \to s\mu^+\mu^-$ after the measurement of R_{K^*}, Phys. Rev. D **96**, 095009 (2017).

[56] A. K. Alok, B. Bhattacharya, D. Kumar, J. Kumar, D. London, and S. U. Sankar, New physics in $b \to s\mu^+\mu^-$: Distinguishing models through *CP*-violating effects, Phys. Rev. D **96**, 015034 (2017).

[57] M. Ciuchini, A. M. Coutinho, M. Fedele, E. Franco, A. Paul, L. Silvestrini, and M. Valli, New Physics in $b \to s\ell^+\ell^-$ confronts new data on Lepton Universality, Eur. Phys. J. C **79**, 719 (2019).